Influence of Catalysts on CO_2-Conversion in Non-Equilibrium Atmospheric Pressure Plasmas

Einfluß von Katalysatoren auf CO_2-Konversion in Nicht-Gleichgewichts-Atmosphärendruckplasmen

Bachelorarbeit

im
Studiengang
“Bachelor of Science”
im Fach Physik

an der Fakultät für Physik und Astronomie
der Ruhr-Universität Bochum

von
Steffen Burkhard Schüttler

aus
Gelsenkirchen

Bochum 2018

Abstract

This thesis deals with the influence of catalysts on CO_2 conversion in a non-equilibrium atmospheric pressure plasma. Manganese dioxide was used as catalyst material and the catalyst surface was in direct contact with the plasma. Fourier transform infrared spectroscopy was used as an in-situ diagnostic for absorption spectra of CO and CO_2. The densities and temperatures of the species were examined by comparison the measured spectra with simulated spectra based on data of the HiTRAN data base. Furthermore, the power characteristic of the plasma was measured.
The conversion rates without catalysts reached values up to 57 %, whereas the conversion rates with catalysts were enhanced and reached values up to 65 %. A dependency of the conversion rate on the loading of the catalysts was found. The higher the loading, the higher the conversion rate. Thereby, loadings of $0.19\,mg/cm^2$, $0.75\,mg/cm^2$ and $3\,mg/cm^2$ were used. Furthermore, the rotational temperatures of CO and CO_2 were in the range of 340 K to 470 K and the vibrational temperature of CO was in the range of 1200 K to 1800 K whereas the vibrational temperatures of CO_2 were around 400 K, 500 K and 800 K, respectively. The rotational as well as the vibrational temperatures of CO and CO_2 did not change their behaviour by adding the catalysts into the plasma system, considering their confidence range. Thus, the effect of the catalysts on the CO_2 conversion is a surface reaction and the presence of catalysts does not change the electronic excitation of the molecules within the plasma.

Zusammenfassung

Diese Arbeit befasst sich mit dem Einfluss von Katalysatoren auf die CO_2 Konversion in einem Nicht-Gleichgewichts-Atmosphärendruck Plasma. Mangandioxid wurde dabei als Katalysatormaterial verwendet und die Katalysatoroberfläche war in direktem Kontakt mit dem Plasma. Ein FTIR-Spektrometer wurde verwendet, um eine in-situ Messung der Absorptionsspektren von CO und CO_2 zu erhalten. Die Dichten und Temperaturen der Spezies wurden durch einen Vergleich der gemessenen Spektren mit simulierten Spektren auf Basis von Daten der HiTRAN Datenbank ermittelt. Zusätzlich wurde die eingekoppelte Leistung in das Plasma gemessen.
Die Konversionsraten ohne Katalysatoren erreichten Werte von 57 %, wohingegen die Konversionsraten mit Katalysatoren höhere Werte von bis zu 65 % erreichten. Eine Abhängigkeit der Konversionsrate von der Beladung der Katalysatoren wurde dabei festgestellt. Je höher die Beladung der Katalysatoren, desto höher die Konversionsraten. Dabei wurden Beladungen von $0.19\,mg/cm^2$, $0.75\,mg/cm^2$ und $3\,mg/cm^2$ verwendet. Des Weiteren lagen die Rotationstemperaturen von CO und CO_2 im Bereich von 340 K bis 470 K und die Vibrationstemperatur von CO im Bereich von 1200 K bis 1800 K wohingegen die Vibrationstemperaturen von CO_2 Werte von 400 K, 500 K und 800 K angenommen haben. Insgesamt waren aber die Rotations- und Vibrationstemperaturen von CO und CO_2 mit und ohne Katalysatoren in ihren entsprechenden Bereichen unter Berücksichtigung ihrer Fehler gleich. Dadurch ist der Effekt der Katalysatoren auf die CO_2 Konversion eine Oberflächenreaktion und das Vorhandensein der Katalysatoren beeinflusst nicht die elektronische Anregung der Moleküle im Plasma.

Contents

1. Introduction

Since industrialisation, the concentration of greenhouse gases in the atmosphere has increased considerably [1]. Therefore, the 'conversion of greenhouse gases (mainly CO_2 and CH_4) into value-added chemicals and liquid fuels is considered as one of the great challenges for the 21st Century' [2]. These value-added chemicals can be used for decentralised storage of renewable energies by converting electrical energy into chemical energy [3].

Plasma technologies are very useful for the conversion of greenhouses gases due to the presence of high energetic electrons. The energetic electrons can active the gas while the overall gas temperature remains near room temperature. This allows CO_2 conversion or dry reforming of CH_4 to take place in the plasma, although these are thermal reactions that require high temperatures [2].

Several plasma technologies have been used for CO_2 conversion such as dielectric barrier discharges [4–6], microwave plasmas [7, 8], gliding arcs [9, 10] and rf discharges [11–13]. Each discharge has its advantages and disadvantages. For example, microwave plasmas have a very high energy efficiency whereas the conversion rate is low [14]. This is due to the trade-off-relationship between conversion rate and energy efficiency.

In order to obtain higher conversion rates while maintaining a high energy efficiency, the combination of plasmas with catalysts can be useful. Different types of catalyst materials have already been tested such as NiO [15], AlO_2 [16] or $BaTiO_3$ and TiO_2 [17]. Each of these studies observed an increase in the conversion rate using the catalysts. On the other hand, Spencer and Gallimore observed a decrease of the conversion rate by using Rh/TiO_2 as a catalyst [18]. Therefore, the choice of the right catalyst is important.

In this thesis, an rf-discharge helium plasma jet developed by Urbanietz et. al will be used for the CO_2 conversion [3]. An in-situ measurement of the system will be performed by Fourier transform infrared spectroscopy (FTIR). This measures absorption spectra of CO and CO_2 within the plasma. The measured spectra will be compared to simulated spectra based on data from the HiTRAN data base to calculate densities and rotational as well as vibrational temperatures of CO and CO_2.

The principle of CO_2 conversion with this plasma has already been thoroughly investigated by Urbanietz et. al [3]. Therefore, it will be examined whether the use of a catalyst improves the system towards higher conversion rates and energy efficiencies. For this purpose, manganese dioxide will be used as the catalyst material. The CO_2 conversion for varying loadings of the catalyst material on the glass plates as well as the effect of sandblasting the glass plates will be investigated. In addition, the energy efficiency and the rotational as well as the vibrational temperatures of CO and CO_2 for the measurements with and without catalyst will be compared.

2. Theoretical background

This chapter deals with a short overview of plasma physics, molecular physics and absorption spectroscopy. The basics of plasma physics are explained and a short overview of different plasmas is given. Molecular physics is examined and the molecules carbon monoxide and carbon dioxide are described. Furthermore, the dissociation of CO_2 by plasmas is described and the characterisation of the process is explained. Finally, the basics of absorption spectroscopy and Fourier transform infrared spectroscopy (FTIR) used as diagnostic method are explained.

2.1 Plasma

A plasma is defined as a quasi-neutral gas, which consists of charged and uncharged particles and shows collective behaviour. In order to define the state of a plasma more precisely, certain conditions can be used [19]:

1. The expansion L of the plasma zone has to be much larger than the Debye length λ_D

$$\lambda_D \ll L. \tag{2.1}$$

   The Debye length is given by

$$\lambda_D = \sqrt{\frac{\epsilon_0 k_B T_e}{n e^2}} \tag{2.2}$$

   with the dielectric constant ϵ_0, the Boltzmann constant k_B, the electron temperature T_e, the electron density n and the elementary charge e. If this condition is fulfilled, there is quasi-neutrality.

2. In order to have collective behaviour, the number of particles N_D within a sphere with the radius of a Debye length must be greater than one

$$N_D \gg 1. \tag{2.3}$$

3. Finally, the product of plasma frequency ω_P and collision frequency τ between charged particles and neutrals has to be greater than one

$$\omega_P \cdot \tau > 1. \tag{2.4}$$

Plasmas can be divided into many categories. One possibility is to divide the plasma by the temperatures of the species within the plasma. In a thermal plasma, the temperatures of all species (electrons, neutrals, ions, ...) are almost equal. This creates a state of equilibrium in a thermal plasma. In contrast, the temperature of the electrons in a non-thermal plasma is much higher than the temperatures of the other species like neutrals or ions. This keeps the overall gas temperature close to ambient temperature. By the difference of the temperatures, a non-thermal plasma

is in a non-equilibrium state [20]. Furthermore, plasmas can be distinguished by their operating pressure. Atmospheric pressure plasmas (APP) are ignited at atmospheric pressure whereas low pressure plasmas (LPP) are operated at low pressure. One advantage of an APP is its simpler design of the plasma chamber compared to an LPP. An LPP requires pumps to generate a low pressure within the plasma chamber. The chamber must withstand the pressure difference and have a correspondingly robust design. Neither is necessary for an APP.

There are several technical configurations such as inductively coupled plasmas (ICP), gliding arc discharges, microwave plasmas and capacitively coupled plasmas (CCP) to generate a plasma. In this experiment, a CCP is used. The setup of a CCP usually consists of two metal plates. These are arranged like the electrodes in a capacitor. An alternating voltage is applied to the plates. This creates an electric field between the plates, which accelerates the charged particles within the plasma. Due to the low mass of the electrons, they are better accelerated and thus they reach higher energies and temperatures.

2.2 Molecular physics

Molecules consist of different atoms which are bound to each other. If energy is supplied to a system consisting of molecules, the energy is distributed to the movement of the molecules and the internal movement of the atoms. The movement of a molecule is a translational movement whereas the movement of the atoms within a molecule is a rotational or vibrational movement.

Each atom in a molecule has three degrees of freedom for its movement. If the molecule consists of N atoms, it has a total of $3N$ degrees of freedom. The translational movement has 3 degrees of freedom due to the movement in all three directions. The rotation takes place around the three main axes of inertia of the centre of gravity. As a result, this movement also has 3 degrees of freedom if its a non-linear molecule. Linear molecules do not rotate around the bound axis and therefore have only 2 degrees of freedom for the rotation. Thus, the vibration of a non-linear molecule has $3N - 6$ degrees of freedom and the vibration of a linear molecule has $3N - 5$ degrees of freedom [21].

To calculate the energies of the translational, rotational or vibrational movement, different models are used. The translational energy E_{trans} corresponds to the kinetic energy of the centre of gravity, whereas the rotational energy E_{rot} is calculated from the model of the rigid rotor. The bond of the atoms in the molecule can be regarded as a spring. This makes it possible to describe the vibrational energy E_{vib} from the model of the harmonic oscillator [22]. The total molecular energy E_{total} results from the addition of these three energies:

$$E_{total} = E_{trans} + E_{rot} + E_{vib}. \tag{2.5}$$

Boltzmann distribution

In a gas mixtures of molecules, the Boltzmann distribution provides an expression for the number of molecules N_i of an energy state E_i as a function of the temperature T of the system. The Boltzmann distribution is given as

$$N_i = N_0 \; g_i \; e^{-\frac{E_i}{k_B T}} \tag{2.6}$$

with the number of molecules in the ground state N_0, the statistical weight g_i of the energy state i and the Boltzmann constant k_B.

The distribution of rotational and vibrational energy levels of an ensemble of molecules can be approximated by the Boltzmann distribution as well. Therefore, a temperature for the rotational and vibrational energy levels can be defined. As the temperature rises, the occupancy of higher levels increases whereas the occupancy of lower levels decreases [22].

CO_2 and CO molecule

The dissociation of carbon dioxide (CO_2) is investigated. Therefore, the two molecules carbon monoxide (CO) and CO_2 are of particular interest.

The CO_2 molecule is a linear molecule and consists of one carbon atom and two oxygen atoms (see figure 2.1 (a)). The CO_2 molecule has $3 \cdot 3 - 5 = 4$ degrees of freedom for the vibration modes, which are shown in figure 2.1. The first vibration mode is the symmetric stretching (figure 2.1 (b)). The oxygen atoms oscillate along the bond axis while maintaining the symmetry of the molecule. The second vibration mode is the bending (figure 2.1 (c)), which is doubly degenerated due to the linear symmetry of the CO_2 molecule. In this process, the oxygen atoms oscillate perpendicular to the bond axis. Finally, the third vibration mode is the asymmetric stretching mode (figure 2.1 (d)). The oxygen atoms also oscillate along the bond axis, but the symmetry of the molecule gets lost due to the inversely oscillation of the oxygen atoms [22].

The different modes, symmetric stretching, bending and asymmetric stretching are characterised by quantum numbers ν_1, ν_2 and ν_3 [23]. These quantum numbers indicate the number of vibration quanta in the corresponding vibration mode.

In general, if the dipole moment of a molecule changes, the causing vibration mode is infrared active. The CO_2 molecule changes its dipole moment by the asymmetric stretching and bending. Therefore, these two vibration modes of the CO_2 molecule are infrared active and can be observed in an infrared spectrum (IR-spectrum). The symmetric stretching does not change the dipole moment and is consequently infrared inactive.

The carbon monoxide (CO) molecule consists of one carbon atom and one oxygen atom. It is a linear molecule as well and has only one degree of freedom for the vibration mode. The oxygen atom can oscillate along the bond axis, which changes the dipole moment of the CO molecule. Therefore the vibration mode of the CO molecule is infrared active as well.

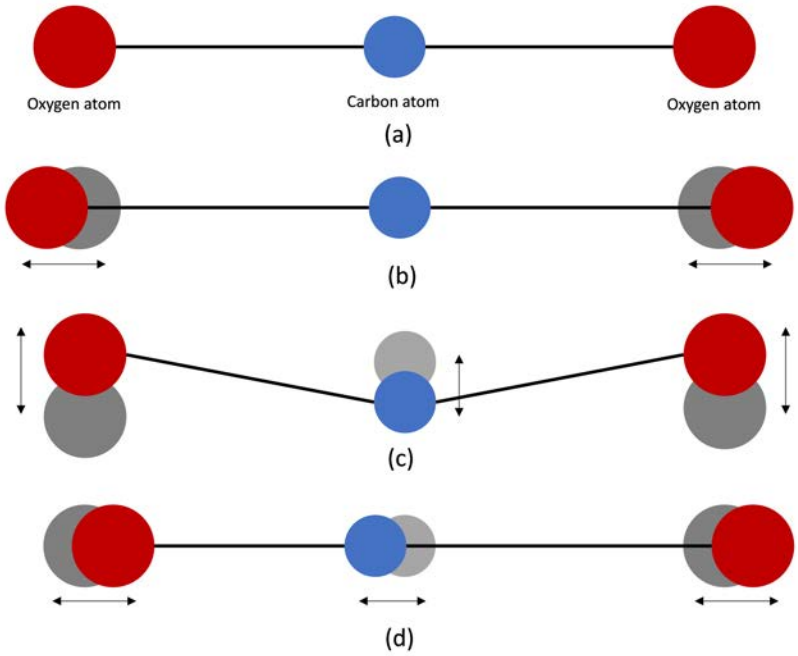

Figure 2.1: Vibration modes of the CO_2 molecule. (a) Structure of the CO_2 molecule: Small circle is the carbon atom, big circles are the oxygen atoms. (b) Symmetric stretching. (c) Bending. (d) Asymmetric stretching. Adopted from [22].

2.3 CO_2 Conversion

This section deals with the dissociation of CO_2 into CO and oxygen. The oxygen can be released into the atmosphere while the CO can be further processed chemically. This dissociation is represented by the following equation

$$CO_2 \quad \rightarrow \quad CO + \frac{1}{2}\, O_2 \;, \quad \Delta H = 2.9\, eV/mol \tag{2.7}$$

with the enthalpy ΔH. The total process starts with the dissociation of CO_2 to CO and atomic oxygen and ends with the recombination of two oxygen atoms to form molecular oxygen [11].

Two main parameters are used to characterise the process of equation (2.7).

1. The conversion rate ϵ describes the proportion of the generated CO to the total number of molecules and is given by

$$\epsilon = \frac{n_{CO}}{n_{CO} + n_{CO_2}} \tag{2.8}$$

with the densities of carbon monoxide n_{CO} and of carbon dioxide n_{CO_2}. At a conversion rate of 100 % all CO_2 molecules are dissociated and only CO is present whereas at 0 % only CO_2 is present.

2. The energy efficiency η is an expression of how the supplied energy is used for the CO_2 conversion and is given by

$$\eta = \frac{\Delta H}{SEI} \cdot \epsilon. \tag{2.9}$$

SEI is the specific energy input which gives an expression for the available energy per molecule inside the plasma by the formula

$$SEI = \frac{P}{\Phi \cdot k} \tag{2.10}$$

with the plasma power P and the total gas flow Φ. The constant k has the value $2.4 \cdot 10^{25}$ and is the Loschmidt-constant.

From equation (2.9) it can be seen that the energy efficiency is inverse proportional to the SEI. As a result, the energy efficiency decreases with increasing SEI. At the same time, as SEI increases, more energy is added to the individual molecules leading to an increase in the conversion rate. Thus, a clear trade-off relationship between the energy efficiency and the conversion rate is present. This relationship is observed in literature by Spencer et al. [11] and Foote et al. [13], for example.

Thermal and non-thermal plasmas are used for the dissociation of CO_2. The energy efficiency of thermal plasmas is limited and only reaches values up to 43 % [20]. In a thermal plasma, the recombination of CO and O is very high whereby CO_2 is recovered. Non-thermal plasmas are used to prevent this. As already mentioned above, the gas temperature in a non-thermal plasma is close to room temperature which makes the recombination lower than in a thermal plasma.

Furthermore, helium is used as forming gas of the plasma. CO_2 is added in a very small admixture (maximum 1 %). As a result, the probability of collisions between the CO_2 molecules is very low. Rather, they collide with He atoms. Likewise, this applies to the CO molecules and O atoms, so that the recombination of CO and O to CO_2 can also be avoided.

2.4 Plasma assisted dissociation

The dissociation of CO_2 in a plasma occurs through different processes. One possibility are the high energetic electrons that drive the dissociation of CO_2 through three different pathways: electron impact dissociation, electron impact ionisation and electron dissociative attachment [5]. The electron impact dissociation forms CO and O from CO_2 by breaking the CO-O bond. This way is the most important for the CO_2 splitting. The electron impact ionisation of CO_2 forms CO_2^+ ions, which will further react with other species to dissociate. At least, the electron dissociative attachment forms CO and O^+.

Furthermore, the high energetic electrons can electronically excite the CO_2 molecules. This excitation also leads to dissociation, but only plays an important role if the reduced electric field $\frac{E}{\rho}$ is very high, which is the case for a low pressure plasma [20].

Since He is used as forming gas of the plasma, another possibility is the dissociation by collisions of CO_2 molecules with metastable He atoms. The high energetic electrons mainly collide with He atoms and generate metastable He atoms and ionised

He^+ atoms. These metastable He atoms may exchange their energy in collisions with other He atoms in the ground state. Furthermore, these excited He atoms collide with CO_2 molecules. This leads to Penning excitation of the CO_2 molecules which may leads either into excitation of CO_2 or into dissociative excitation of CO_2 to $CO^+ + O$ [3].

2.5 Catalysis

The effect of catalysts on the CO_2 dissociation will be investigated in this thesis. The following describes the concept of the catalyst and its properties.

The first catalytic reactions were discovered at the end of the 18th century. These includes the saccharification of starch and the decomposition of ammonia and hydrogen peroxide [24]. Since the 19th century, catalysis plays an important role in chemistry.

According to Ostwald 'catalysts are substances that accelerate the rate of chemical reactions without themselves being consumed during the reactions' [25]. Thereby, positive and negative catalysts can be defined. Catalysts that accelerate reactions are referred to as positive catalysts, whereas negative catalysts slow down the reactions [26].

Catalyst are also differentiated by their aggregate states in comparison to the reacting medium. A homogeneous catalyst has the same aggregate state as the reacting medium. In the case of heterogeneous catalysts, the catalyst and the reacting medium have a different aggregate state. Heterogeneous catalysts are mainly solids and the reacting medium is a gas or a liquid.

Many organic catalysts such as proteins or enzymes are present in nature. In contrast, the conventional chemistry mainly uses inorganic catalysts. Some of these catalysts already have catalytic effects due to their acidic and basic properties. However, most catalysts are metals such as Cu, Fe, Co, Ni, Cr, Mo, and Mn or metal oxides like MgO, MnO, CoO and NiO. These metals are used to accelerate hydrogenation reactions. Precious metals such as Ag, Pt and Pd are also used as catalysts and serve to accelerate hydrogenation reactions.

Metallic catalysts often consist of two components, the metal component and a supporter. As supporters, aluminium oxides, aluminium silicates, silica, kaolin, bentonites or carbons are used. The supporters allow a high distribution of the metals on the surface and ensure a thermally stable distribution [26].

The main properties of a catalyst are the specific surface area, the porosity and the texture of the catalyst. The specific surface area is given by the surface size per mass unit of the solid. Porosity is the proportion of the cavity volume and the total volume of the catalyst and the texture gives an expression of the size, size distribution and shape of the pores. In addition, the loading of the catalyst on the surface is an important property. This indicates how much catalyst material is deposited on the surface. In this thesis, a metal oxide catalyst with different loadings is used (see below).

2.6 Plasma catalysis

Plasma catalysis is the combination of a plasma with a catalyst. Neyts and Bogaerts have performed research on this topic and they summarise the most important interactions between a plasma and a catalyst [5]. These interactions are shown in figure 2.2 and are based on various experiments described in literature.

Effects of catalysts on plasmas

The electric field enhancement is caused by the roughness of the catalyst surface. It is a physical effect and directly affects the electron energy distribution. Therefore, the electron impact dissociation is changed which eventually changed the conversion rate. The higher electric field on the catalyst surface also forms strong microdischarges on the catalyst surface. These microdischarges change the electron energy distribution as well.

If the catalyst is placed directly inside the plasma, increased surface discharges can occur whereby the ionisation rate is increased and more reactive species are created. This results in more reactions between CO_2 molecules and reactive species, which eventual increases the dissociation of CO_2, for example.

Furthermore, the catalyst can adsorb pollutants from the plasma. In this way, the pollutants have a longer residence time in the plasma and can therefore have an increased influence on the plasma. However, this effect depends on the extent of contamination of the incoming gas.

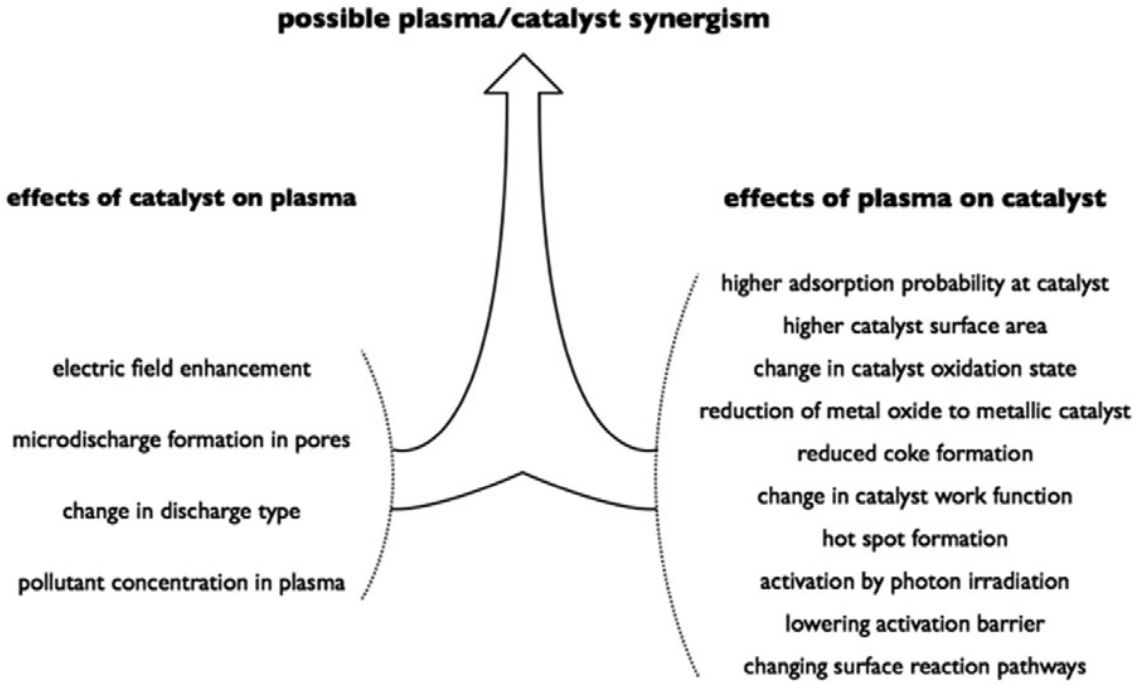

Figure 2.2: Possible plasma catalysis synergism [5].

Effects of plasmas on catalysts

The catalyst is in direct contact to the plasma, which changes the physiochemical properties of the catalyst by the plasma. First, the catalyst can have a higher adsorption probability due to the change of the electric surface properties by the plasma. The plasma can also lead to the formation of smaller nanoparticles on the surface of the catalyst. Through these smaller nanoparticles, the total surface area of the catalyst is increased.

The discharge can change the oxidation state of the catalyst as well. This may occur either under the influence of a high voltage or through the interaction with reactive oxygen species. If the catalyst is a metal oxide, the change of the oxidation state may reduce the catalyst from a metallic catalyst with oxygen to a pure metallic catalyst. Furthermore, the coke formation on the catalyst surface is reduced, leading to a lower deactivation of the catalyst.

Additionally, there can be a change in the work function of the catalyst, which is defined as the energy required for an electron to be removed from the surface of the catalyst. The work function is strongly affected to the presence of voltage and current, which can change the electron extraction potential to lower values.

Relating to the electric field enhancement described above, strong microdischarges can be created in the area of pores of the catalyst surface. These microdischarges create local ares of higher temperatures, so called hot spots. Due to the higher temperature of the hot spots, the catalyst can be activated thermally or the chemical reaction can be improved.

Moreover, the photons inside the plasma can promote electrons from the valence band to the conduction band of the catalyst leading to a higher activation of the catalyst. Besides that, the activation barrier for surface reactions between catalyst and plasma is lower due to the excited (especially vibrationally) species in a plasma. Additionally, the reaction pathways on the catalyst will also be changed. The plasma consists of reactive particles like ions, electrons, atoms, radicals and electronically or vibrationally excited species. These species react differently with the catalyst and therefore the reaction pathways of a plasma-catalysis system can be very different to a thermal catalysis system.

All these different effects of a plasma on the catalyst and vice versa ensure that the reactions taking place within the system are modified. This should eventually lead to an increase in conversion and energy efficiency with the aid of a catalyst.

2.7 Absorption spectroscopy

In order to investigate CO_2 conversion, it is necessary to be able to examine the species within the plasma. Various diagnostics such as emission spectroscopy or mass spectroscopy are available for this purpose. In this thesis, absorption spectroscopy with Fourier transform infrared spectroscopy (FTIR) is used to analyse the plasma.

Quantum mechanics describes the absorption as the transition of an energy level i to a higher level j via the Einstein coefficient for the absorption B_{ij}. The change in the number of particles N_j in the higher energy level j is described by

$$\frac{dN_j}{dt} = -N_i B_{ij} \rho(\nu) \tag{2.11}$$

with the number of particles N_i in the energy level i and the Planck's law $\rho(\nu)$ [27]. The numbers of particles of the two energy levels are given by the Boltzmann distribution according to equation (2.6).

The absorption is induced by electromagnetic radiation (infrared light). Thus, the transition of the energy levels depends on the Planck's law, which determines the spectral densities of the electromagnetic radiation. Planck's law is given by

$$\rho(\nu) = \frac{8\pi h\nu^3}{c^3} \frac{1}{e^{\frac{h\nu}{k_B T}} - 1} \tag{2.12}$$

with the frequency ν of the light, the speed of light c, the Boltzmann constant k_B and the temperature T.

Additionally, the connections between the Einstein coefficient for the absorption B_{ij} and those for stimulated emission B_{ji} and spontaneous emission A_{ij} are given by

$$B_{ij} = \frac{g_i}{g_j} B_{ji}, \tag{2.13}$$

$$B_{ij} = \frac{c^3}{8\pi h\nu^3} A_{ik}. \tag{2.14}$$

With the same statistical weights of the energy levels i and j, the Einstein coefficients for absorption and stimulated emission are equal [21].

Furthermore, the intensity of the absorbed light in an absorbing medium is reduced. This process is described by the Lambert-Beer law

$$I = I_0 \, e^{-\alpha l} \tag{2.15}$$

where I_0 is the intensity of the light source, α is the absorption coefficient and l is the path length of the light within the absorbing medium.

The absorption coefficient can be represented by the concentration of the absorbing medium c and the molar absorption coefficient ϵ

$$\alpha = \epsilon \, c. \tag{2.16}$$

By measuring the light intensities before and after the absorbing medium, the Lambert-Beer law can be used to determine the concentration of the absorbing medium [28].

Fourier transform infrared spectroscopy

As discussed above, CO and CO_2 are infrared active molecules. To determine the densities of CO and CO_2 inside the plasma reactor, the Fourier transform infrared spectroscopy (FTIR) is used. The FTIR is based on a Michelson interferometer. The setup of an FTIR and the sample compartment with the pathway of the infrared light is shown in figure 2.3. It consists of a beamsplitter and two mirrors. One of the mirrors is fixed, while the other mirror is movable. The infrared light beam passes the beamsplitter and is divided into two beams. One beam runs to the fixed mirror, the other one runs to the movable mirror. Both beams are reflected from the respective mirror back to the beamsplitter where they recombine and interfere. The interfered beam passes through the plasma chamber and reaches the detector where it is focused by a lens.

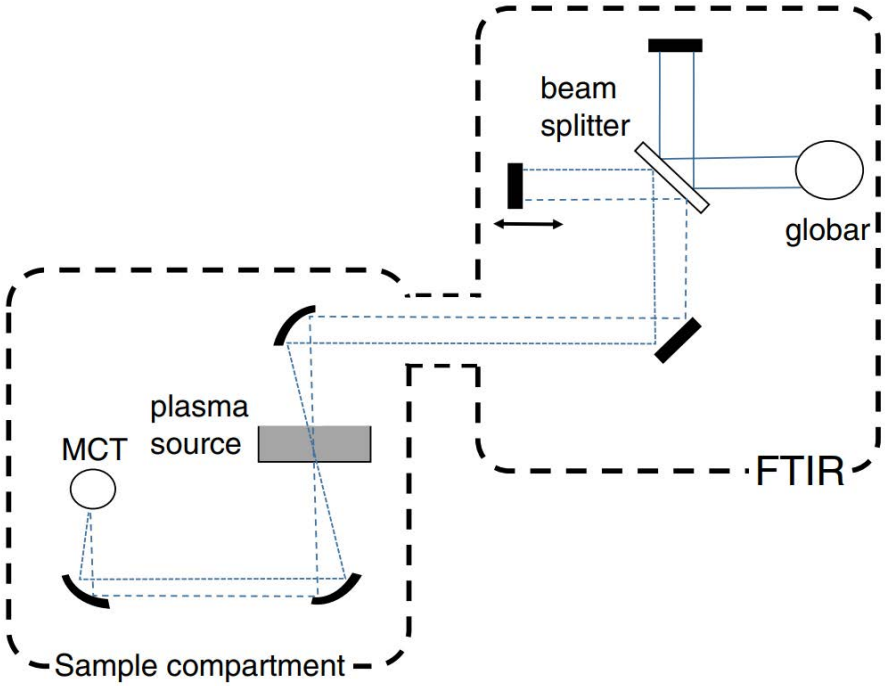

Figure 2.3: Scheme of an FTIR spectrometer with a Michelson interferometer and the sample [3].

The FTIR records an absorption spectrum as a function of the mirror position z. But a dependence of the spectrum on the wavenumber $\bar{\nu}$ is required. To obtain these from the mirror position, a Fourier transformation is applied

$$I(\bar{\nu}) = \sum_{n=0}^{N-1} I(z) e^{-2\pi i n k/N} \tag{2.17}$$

with the total number of mirror steps N, $k \in \mathbb{Z}$ and the intensity of the absorption spectrum depending on the mirror position $I(z)$. This results in the absorption spectrum as a function of the wavenumber with the intensity $I(\bar{\nu})$.

3. Experimental setup

This chapter deals with the experimental setup. The plasma chamber with power and gas supply as well as the power measurement is described. Furthermore, the FTIR measurement with the measured and modelled spectra is explained. The use and production of the catalysts are also described.

3.1 Plasma setup

Figure 3.1 shows the cross section of the plasma chamber from the side (left) and from the front (right). The plasma chamber consists of an aluminium main body with different recesses on the sides. The recesses on top and bottom of the chamber are used for the electrode holders which consist of an aluminium body, a macor insulation and a copper electrode. The electrodes have an area of 26 mm × 13 mm and a thickness of 0.5 mm. Glass plates are attached to the electrodes to protect them from the plasma. Unwanted arcing effects are also avoided due to the glass plates serving as dielectric. The distance between the two glass plates is 1 mm whereby the plasma volume is confined to 26 mm × 13 mm × 1 mm. One electrode is connected to an rf-generator via a matching system while the other electrode is grounded.

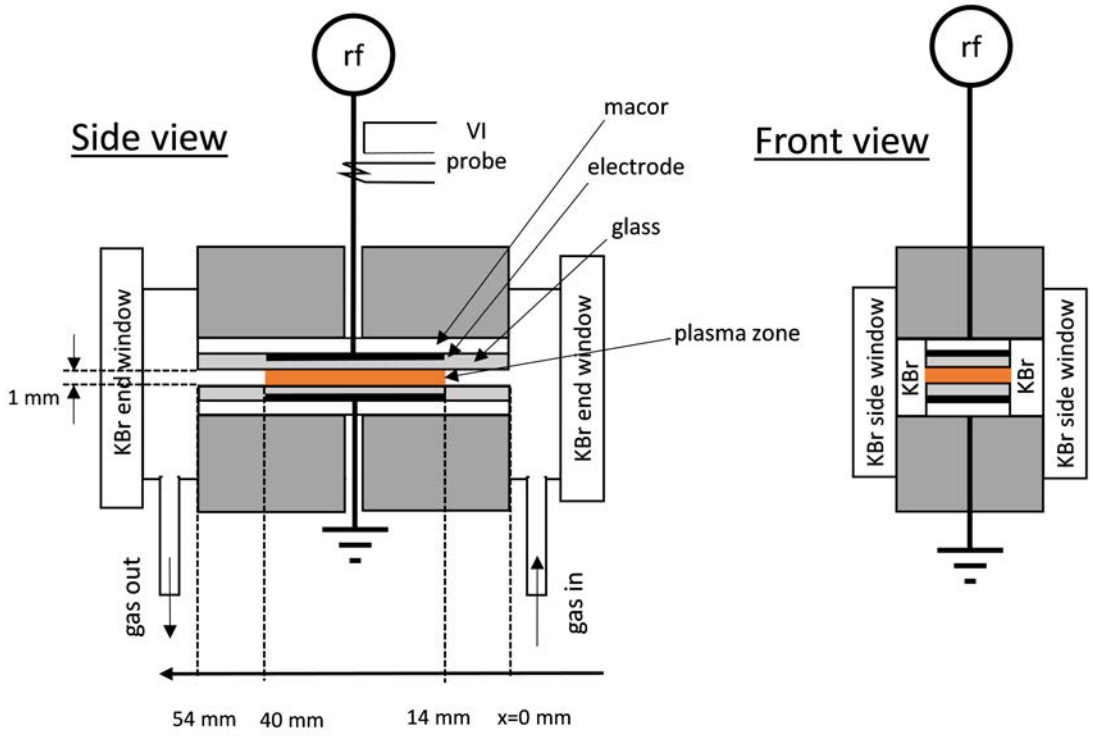

Figure 3.1: Cross section of the plasma chamber. Adopted from [3].

The gas volume is limited by potassium bromide (KBr) windows. These windows are transparent for infrared light, which is necessary for the diagnostics (see below). The KBr end windows (see fig 3.1 left) allow a view into the plasma chamber in direction of the gas flow while the side windows (see fig 3.1 right) allow a view perpendicular to the gas flow. Additionally, two small KBr windows are inserted between the macor layer and the KBr side windows. These ensure that the entire gas flows between the electrodes and that no gas gaps occur laterally of the electrodes. Thus, only the plasma is observed if the infrared light beam is incident from the side.

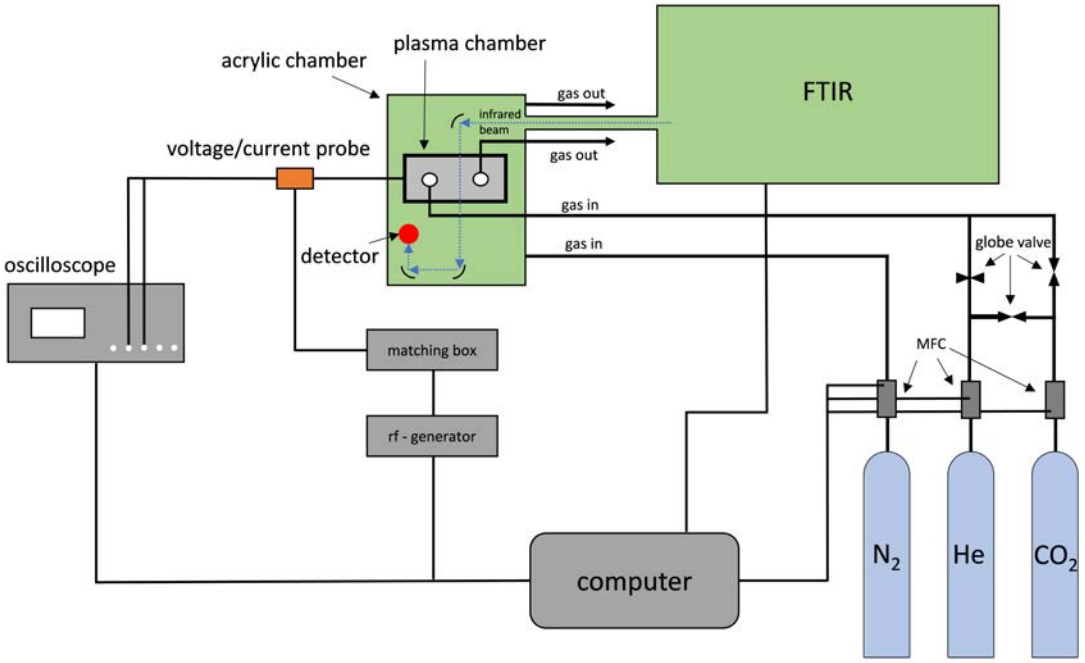

Figure 3.2: Scheme of the experimental setup.

The experimental setup of the plasma chamber with gas and power supply is shown in figure 3.2. The plasma is operated with a gas mixture of helium and CO_2. Mass flow controller (MFC) are used to control the gas flow and are regulated by a LabView program. The helium flow varies with certain CO_2 admixtures of 0.25 %, 0.5 % and 1 %. In the case of a helium flow of 250 sccm, these admixtures correspond to a CO_2 gas flow of 0.625 sccm, 1.25 sccm and 2.5 sccm, for example.

Furthermore, the plasma chamber is connected to an rf-generator (RFG100-13 by Coaxial Power Systems Ltd.) which operates at a frequency of 13.56 MHz and powers up to 100 W. A matching System (MMN-100-13 by Coaxial Power Systems Ltd.) is used to adjust the plasma impedance to the 50 Ω exit impedance of the generator to avoid back-reflected waves.

A voltage and current probe is used to measure the power dissipated in the plasma. The probe consists of a 2.2 Ω resistor and a voltage pick-up probe (see figure 3.3). Both probes were connected via an BNC cable to an oscilloscope (DPO 3014, Tektronix, 2.5 Gs/s, 100 MHz, 256 averages) to observe the voltage and current behaviour in time. A python script reads out the voltage, current and the phase shift between the two and calculates the plasma power.

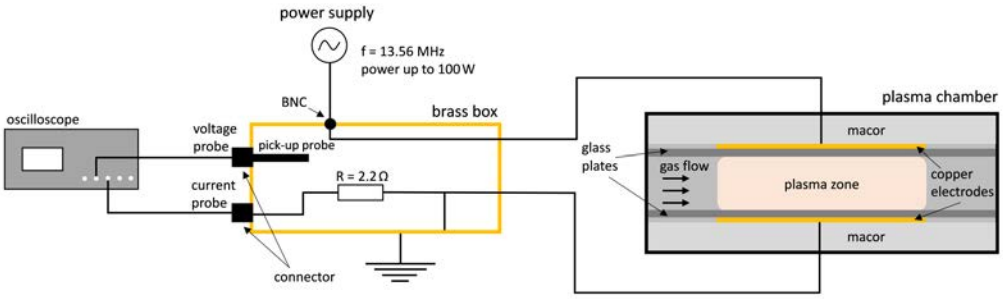

Figure 3.3: Scheme of the probe for the power measurement. Adopted from [29].

3.2 FTIR measurement

FTIR measurement is used as the diagnostic method. To avoid background noise, the plasma chamber is surrounded by an acrylic chamber, which is continuously flushed with nitrogen (flow rate of 20 slm) during the measurements (see figure 3.2). The beam path of the FTIR runs inside the acrylic chamber (see figure 3.4). Thus, mainly the infrared inactive gas nitrogen is still located in the beam path. Some water and CO_2 absorption lines are still visible in the background spectrum. If a background spectrum is recorded without a plasma, the absorption spectrum within the plasma chamber can be recorded. Therefore, the logarithm of the intensity of the background measurement divided by the intensity of the sample measurement is used [30]. This results in an in-situ absorption spectrum of the plasma. The infrared beam is detected by a liquid nitrogen cooled HgCdTe-detector.

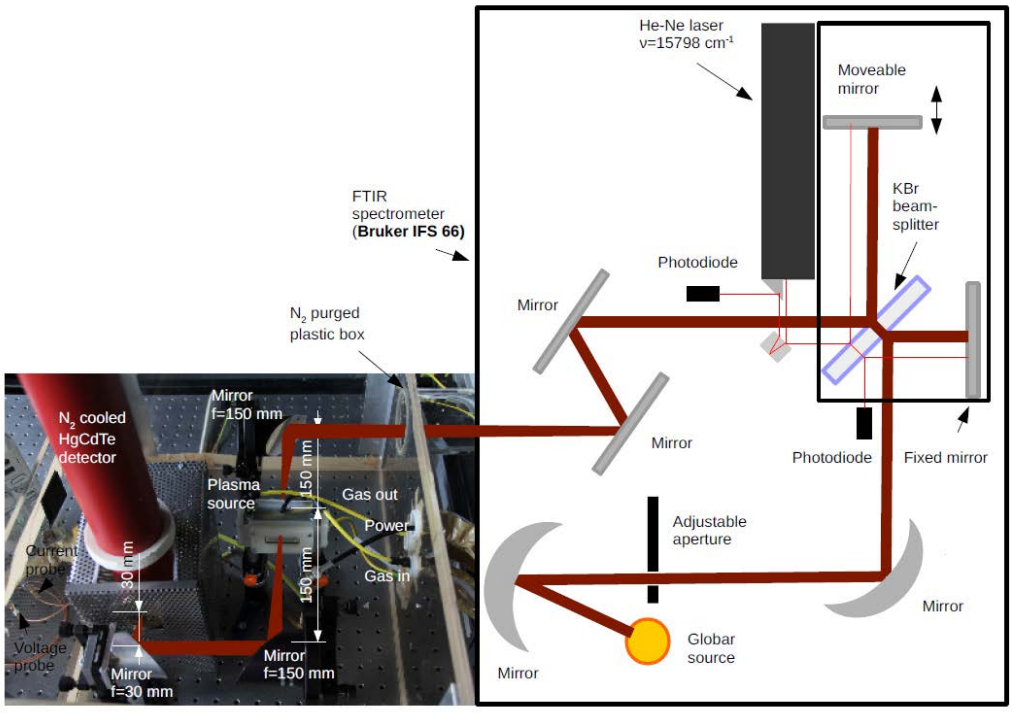

Figure 3.4: Setup of the FTIR spectrometer (Bruker IFS 66/S) [29].

The position of the moving mirror is determined by a helium neon laser with a wavelength of 633.4 nm. The laser beam is also divided into two beams and the beams are reflected at the two mirrors as well.
The interference of the two beams can be constructive or destructive. In order to obtain constructive interference, the path difference Δl must be a multiple of the wavelength

$$\Delta l = k\lambda \tag{3.1}$$

with the wavelength λ and $k \in \mathbb{N}$. Destructive interference occurs for

$$\Delta l = (2k - 1)\lambda. \tag{3.2}$$

The position of the mirror can be determined by the interference of the two laser beams using equation (3.2). This creates an absorption spectrum depending on the position of the mirror. As describes above, a Fourier transformation converts the dependence on the mirror position into a dependence of the absorption spectrum on the wavenumber.

Furthermore, the frequency resolution of the FTIR is given by

$$\Delta\nu = \frac{1}{N\Delta l}. \tag{3.3}$$

Thus, the resolution can be enhanced by the path difference Δl and the total number of mirror steps N. The path difference is determined by the FTIR. The number of mirror steps can be set on the control program of the FTIR. A setting of 100 scans has proven to be sufficient to get a good signal with an acceptable waiting time.

Two absorption spectra are shown in figure 3.5 as an example. They were recorded with a He gas flow of 250 sccm and CO_2 admixtures of 0.25 % and 0.5 %, respectively. The generator power in both cases was 50 W. The corresponding plasma powers are 1.72 W for the small admixture and 1.45 W for the higher admixture.

The absorption bands for CO and CO_2 are clearly visible in the spectra. At a wavenumber of $\nu_1 = 2149\,\mathrm{cm}^{-1}$, the stretching vibration of CO is present whereas at $\nu_3 = 2340\,\mathrm{cm}^{-1}$ the asymmetric stretching of CO_2 is visible. In comparison, the absorption lines for CO and CO_2 in the left spectrum are significantly larger due to the higher admixture of CO_2. Furthermore, the baseline in the two spectra is shifted due to heating of the plasma chamber. The spectra in the experiment show that the baseline shifted to higher values for higher generator powers. As the generator power increases, the system heats up more and the baseline shifts accordingly.

The absorption spectra are modelled to determine the densities and the rotational as well as the vibrational temperatures of CO and CO_2 from the spectra. In order to model the absorption transitions, the wavenumbers with the corresponding Einstein coefficients are taken from the HiTRAN data base. The calculation of the absorption spectra follows six steps including the rotational and vibrational distribution, line strengths, line broadening, optical transmission and instrumental broadening. The total calculation follows the code from Klarenaar et al. [31].

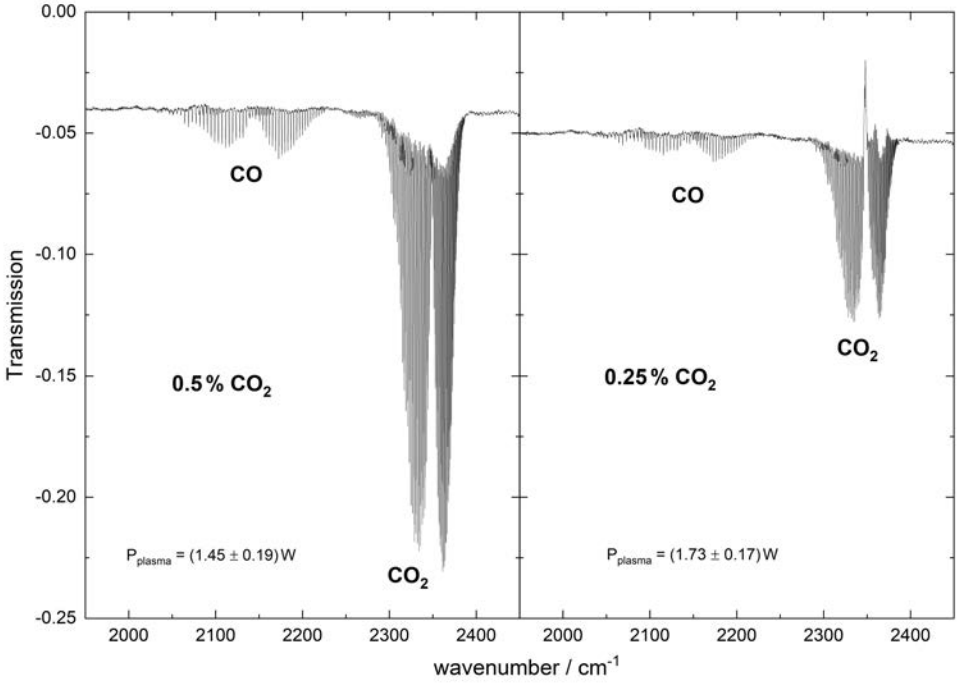

Figure 3.5: Absorption spectra for 250 sccm He with 0.5 % CO_2 (left) and 0.25 % CO_2 (right) at a generator power of 50 W. The corresponding plasma powers are 1.72 W for the small admixture and 1.45 for the higher admixture.

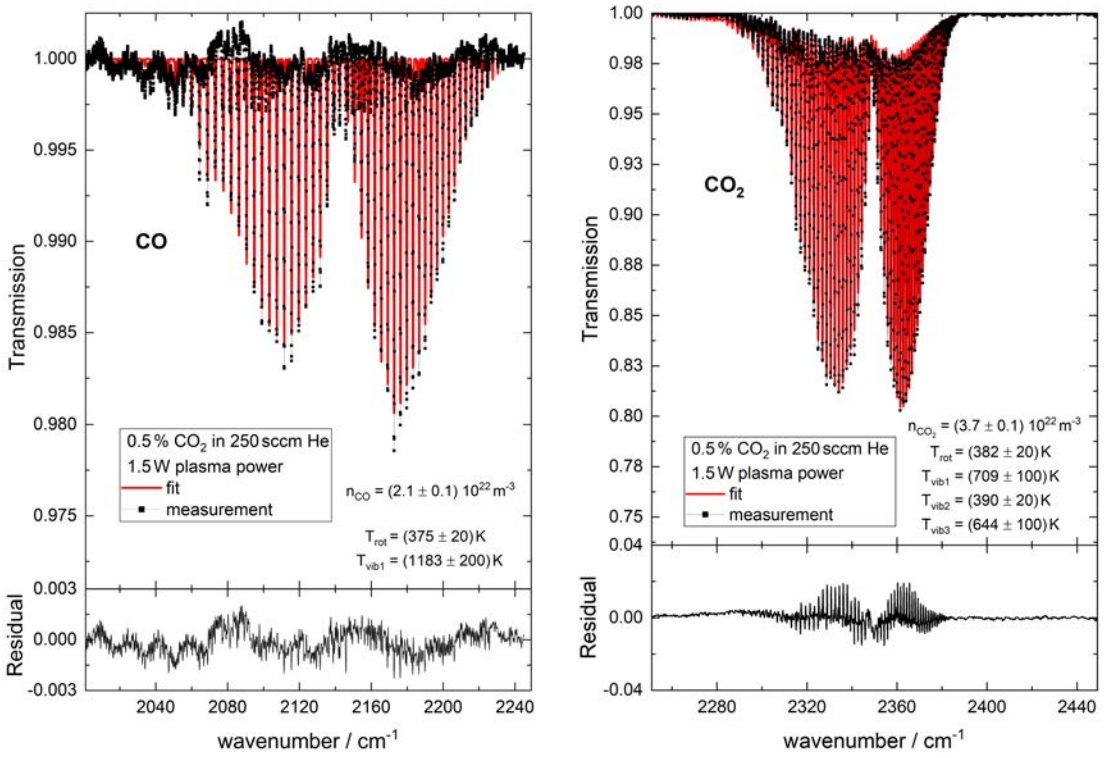

(a) CO (b) CO_2

Figure 3.6: Absorption spectra of CO and CO_2 for 250 sccm He with an CO_2 admixture of 0.5 % at a generator power of 50 W resulting in a plasma power of 1.5 W.

In figure 3.6, the measured and calculated absorption spectra for CO and CO_2 are shown as examples. The upper panels show the calculated and measured absorption spectra whereas the lower panel shows the residuum between the measurement and the model. The corresponding densities and temperatures of the models are also shown in the figure.

Both models are in good agreement with the measurements. The absolute scale of the residuum in both cases corresponds to 20 % of the maximum absorption signal. The shifted baselines of the measurements were adjusted to the model. It should be noted that a curve is recognisable in the absorption spectrum of CO. This is caused by interference of the infrared light on the small KBr windows. If the windows are not properly fixed, they can move and are not parallel to each other. As a result, the infrared light can interfere and the curve is formed in the spectra. During experiments with correctly mounted windows, the interference could not be detected. However, the modelling works despite the interference as the curve is also visible in the residuum. In order to obtain the correct values, the densities and temperatures must be varied until only the curve in the residuum is recognisable.

3.3 Catalysts

Catalysts are used to influence the chemical reactions in the plasma chamber. In the following, the integration of the catalyst into the plasma chamber and the production of the catalysts are described.

In this experiment, manganese dioxide (MnO_2) is used as material for the heterogeneous catalysts. This is obtained by the proportioning reaction of $KMnO_4$ and $Mn(NO_3)_2$

$$2MnO_4^- + 3Mn^{2+} + 4OH^- \longrightarrow 5MnO_2 \downarrow + 2H_2O. \tag{3.4}$$

The chemists from the chair of industrial chemistry at the Ruhr-University Bochum use this reaction to produce the MnO_2. The exact procedure can be found in [32].

The catalyst surface should be in direct contact with the plasma. To achieve this, the catalyst material is applied to the surface of the glass plates which are mounted on the electrodes (see fig. 3.7). In this way, the plasma is in direct contact with the catalyst surface.

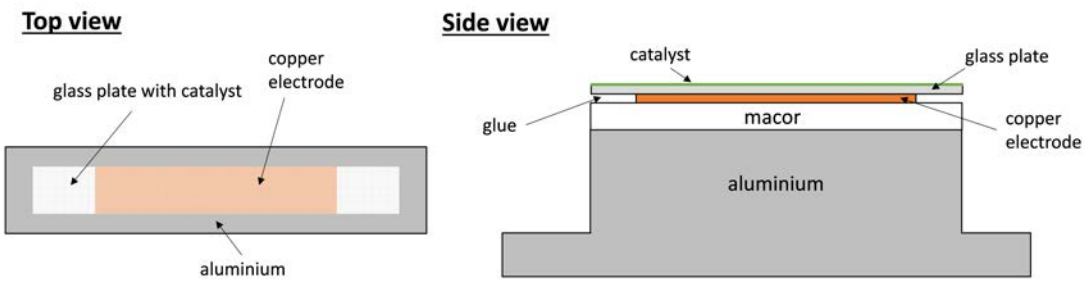

Figure 3.7: Setup of the electrode holder with glass plate and catalyst.

A spray coating system is used to coat the glass plates with the catalyst material. The setup (left) and a picture (right) of the spray coating system is shown in figure 3.8. The catalyst material is located in a suspension. Water and isopropanol in the ratio of 1:1 are used as the suspension liquid. This ensures slow sedimentation and good evaporation. The suspension is stored in a container with a magnetic stirrer. A piston pump transports the suspension to a spray head. The spray head is used to apply the material on the surface and is movable in x- and y-direction. In order to obtain a reproducible coating, the glass plates are heated to 200°C during coating on a hot plate. The distance between the spray head and the hot plate is fixed to 17 cm. The loading of the catalyst material on the surface is adjusted by varying the distance between the spray points. Additionally, the suspension is fogged with compressed air for the application. Furthermore, the glass plates are cleaned with fully de-acidified water and acetone before coating.

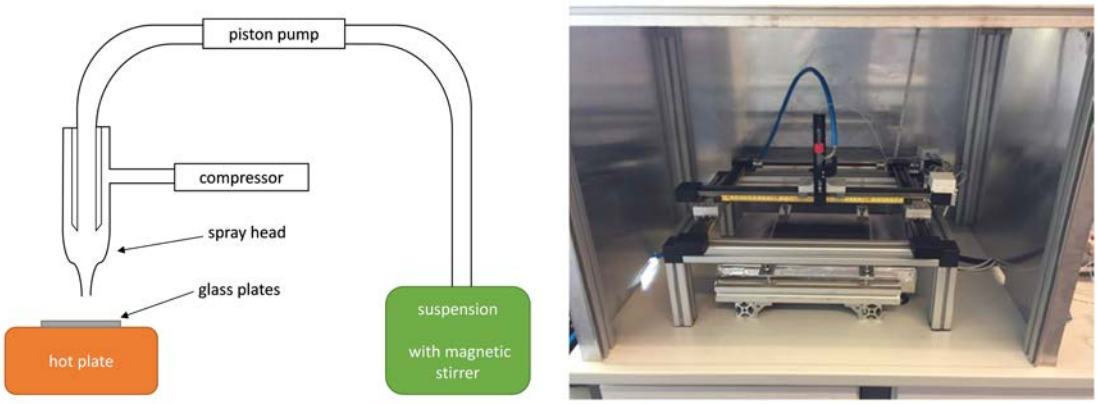

Figure 3.8: Scheme (left) and picture (right) of the spray coating system. Adopted from [32].

During coating, it was observed that the material was carried outwards by the compressed air and did not adhere to the glass surface. To prevent this, the glass plates are treated with a sandblast of a mixture of sodium glass and corundum before coating. This makes the surface rougher and the material can adhere better.

The applied volume per spray point is adjusted on a computer to control the spray coating system. It turned out that the actual spray volume is 3 times higher than the adjusted spray volume [32]. The adjusted and actual loadings of the catalyst material on the glass plates are listed in table 3.1.

Table 3.1: Adjusted and actual loadings of the catalyst material on the glass plates.

adjusted mg/cm^2	actual mg/cm^2
0.063	0.19
0.25	0.75
1	3

The sandblasted and non-sandblasted glass plates with and without catalyst used in this experiment are shown in figure 3.9. The non-sandblasted glass plate without catalyst (1) is transparent. In the figure, it appears brownish due to the background. A brown sheet was used because on a white sheet the difference between the non-sandblasted and the sandblasted glass plates was not recognisable. The surface of the sandblasted glass plate (2) appears whitish compared to the non-sandblasted (1) due to the rougher surface. The catalyst material is clearly visible on the glass plates (3) to (6). On the sandblasted glass plates ((4) to (6)) the catalyst material is distributed homogeneously whereas on the non-sandblasted plates (3) the material is distributed unevenly. Areas with much and less catalyst material have formed on the non-sandblasted plates (3). In addition, the glass plates with higher loads become darker and darker as more catalyst material is deposited on the surface.

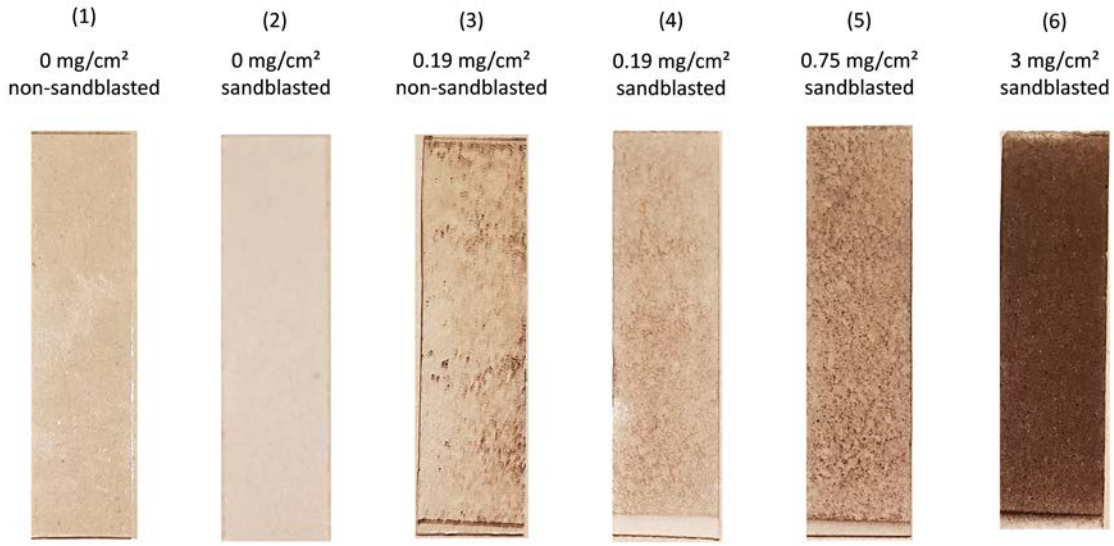

Figure 3.9: Pictures of the glass plates.

4. Results and discussion

This chapter describes the results and the discussion of the measurements. The effect of the additional small KBr windows is explained. Afterwards, the coupled plasma power into the plasma system is examined to get an overview of the behaviour of the plasma. Furthermore, the time evolution of two catalysts is analysed and the conversion rates for each catalyst are presented. The energy efficiency of the conversion as well as the rotational and vibrational temperature behaviour of CO and CO_2 are shown and explained. Finally, the performance of the plasma catalysis system is discussed.

4.1 Effect of the small KBr windows

The setup of the plasma chamber with the additional small KBr windows is described in chapter 3 and figure 3.1. Urbanietz et al. discussed the complex flow pattern of the helium gas flow without these small windows [3]. Without the small KBr windows, gas gaps are formed in which the gas accumulates. This gas does not enter the plasma zone and therefore CO_2 is not dissociated in this region. As a result, even at a 100 % conversion rate in the plasma, the measured conversion rate are much lower. To prevent the gas gaps, the two small KBr windows are used in this experiment.

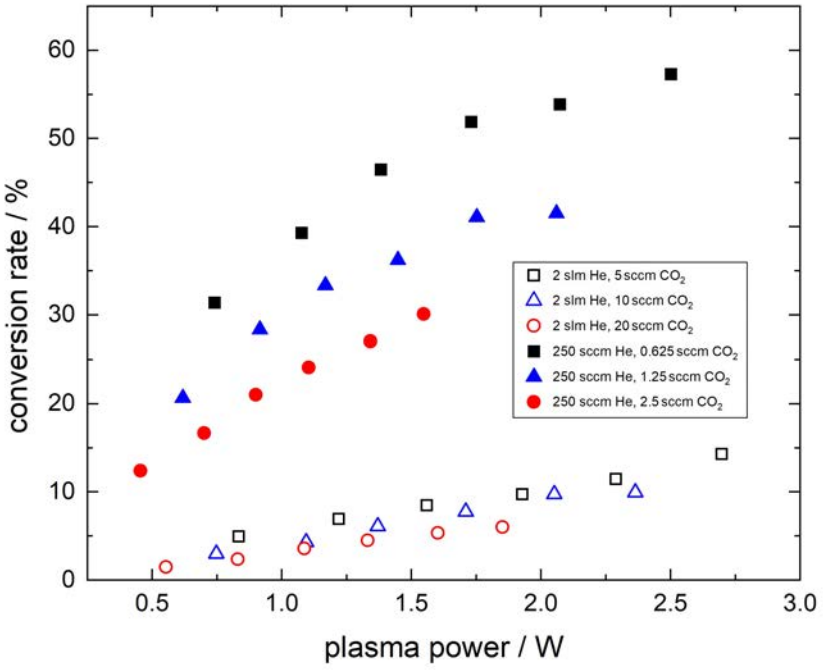

Figure 4.1: Conversion rate as a function of plasma power for a slow (250 sccm) and a fast (2 slm) helium flow with CO_2 admixtures of 0.25 %, 0.5 % and 1 %.

Without the small KBr windows, Urbanietz et al. reached conversion rates of 30 %, 25 % and 15 % for the CO_2 admixtures of 0.25 %, 0.5 % and 1 %, respectively at a gas flow of 2 slm [3]. The conversion rates with the small KBr windows for the three CO_2 admixtures at the same helium flow are shown in figure 4.1. In this case the conversion rate is 15 % for 0.25 % CO_2 admixture, 10 % for 0.5 % CO_2 admixture and 5 % for the highest CO_2 admixture of 1 %. The conversion rates are lower compared to Urbanietz et al. because the residence time of the gas in the plasma chamber is lower. The residence time τ is given by

$$\tau = \frac{V}{\Phi} \tag{4.1}$$

with the volume V and the gas flow rate Φ.

Inserting the small KBr windows reduces the volume resulting in a lower residence time. Due to the lower residence time, the conversion rates are also lower. The flow pattern provides a velocity reduction by a factor of 8 for the setup with small KBr windows compared to the setup without small KBr windows. Therefore, the gas flow of helium is reduced to 250 sccm. The conversion rates for the lower gas flow reach values up to 57 % for the CO_2 admixture of 0.25 %, 40 % for the admixture of 0.5 % and 30 % for the admixture of 1 %. In this thesis, further measurements are performed with the lower helium gas flow of 250 sccm with three CO_2 admixtures of 0.25 %, 0.5 % and 1 %.

4.2 Plasma behaviour due coupled plasma power

In this section, the power coupled into the plasma is investigated to characterise the plasma. For each admixture, the generator power varies from 20 W to 70 W in 10 W steps. A python script measures the plasma power faster than a second. Approximately, the plasma power is measured 650 times over a complete absorption spectrum measurement. In the evaluation, the mean value is calculated from these data.

The coupled plasma power as a function of the generator power for the smallest CO_2 admixture of 0.25 % is show in figure 4.2. The plasma powers are shown for the sandblasted and non-sandblasted glass plates as well as for each catalyst. It can be seen that the plasma power increases linearly with the generator power in each case. However, there is a slight difference between the measurements with catalyst and sandblasted glass plates compared to the non-sandblasted glass plates without catalyst. At a generator power of 40 W, all plasma powers are almost equal at a value of 1.5 W. For higher generator powers, the plasma powers for measurements with catalysts and the sandblasted glass plates are larger compared to the non-sandblasted glass plates. For lower generator powers the plasma powers are lower or equal. These are lower for the sandblasted glass plates and for the catalysts with the smallest loading of 0.19 mg/cm^2 on non-sandblasted glass plates and the loading of 0.75 mg/cm^2 on sandblasted glass plates. The plasma powers are almost equal for the catalysts with the smallest loading of 0.19 mg/cm^2 and the highest loading of 3 mg/cm^2 on sandblasted glass plates.

In each experiment with the smallest CO_2 admixture, the plasma ignited homogeneously over the entire electrode area. This was visually observed and is also evident from the linear increase in plasma power.

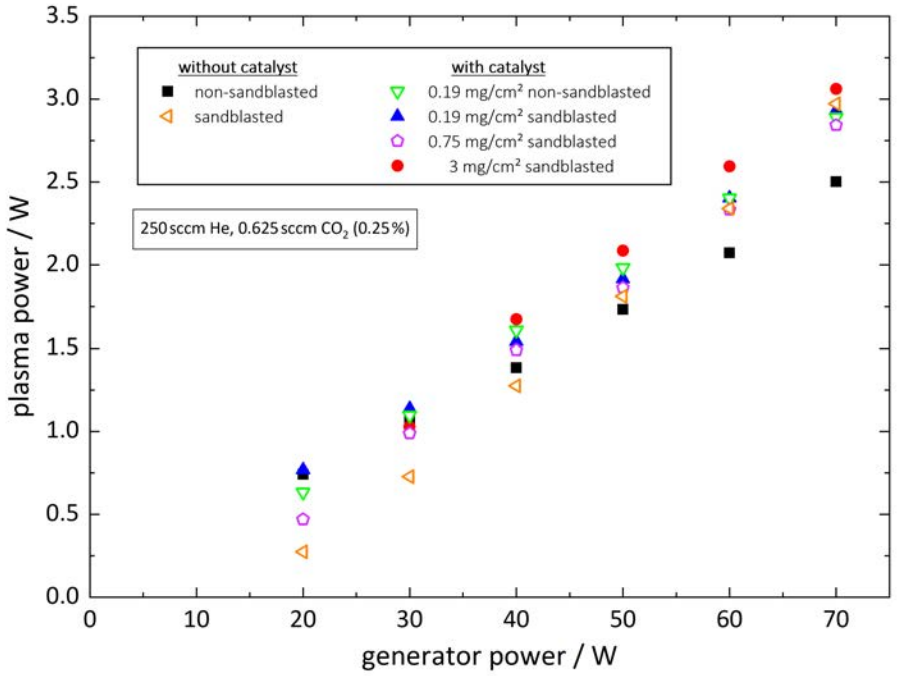

Figure 4.2: Plasma power as a function of the generator power for a He flow of 250 sccm and a CO_2 admixture of 0.25 %.

The coupled plasma powers for the medium and high CO_2 admixtures are shown in figure 4.3. For sake of clarity, only three measurements were selected: without catalyst on sandblasted as well as on non-sandblasted glass plates and the measurement with catalyst with the highest loading of 3 mg/cm^2 on sandblasted glass plates. The plasma power of the other catalysts (0.19 mg/cm^2 on sandblasted as well as on non-sandblasted glass plates and 0.75 mg/cm^2 on sandblasted glass plates) show the same behaviour for the medium and high CO_2 admixture as described in the following.

It can be seen that the plasma power of the reference measurement without catalyst on non-sandblasted glass plates increases linearly in both cases. On the other hand, the profiles of the measurements without catalyst on sandblasted glass plates and with catalyst (3 mg/cm^2) on sandblasted glass plates show a non-linear behaviour. For low generator powers such as 20 W, 30 W and 40 W for the high CO_2 admixture (see fig. 4.3b), the plasma power of the two is close to zero. At a generator power of 40 W for the medium CO_2 admixture (fig. 4.3a) and 50 W for the high CO_2 admixture (fig. 4.3b), the plasma power of the two increases abruptly.

This behaviour could also be observed visually. The plasma did not ignite homogeneously at low generator powers or could not be ignited at all. In some cases, the plasma ignited only on one side of the electrodes and not on the entire area. This is due to the fact that the electrodes are arranged slightly offset from each other. One of the electrodes is a little narrower and not soldered exactly in the middle of the cable. This results in an offset on one side, whereby the plasma ignites not homogeneously for the 0.5 % and 1 % CO_2 admixture. The plasma was less than half formed so that the plasma power for these cases is coupled in a different way. For the generator powers at which the plasma powers jump, the plasma forms in the entire chamber. Thereby, the coupled plasma power increases abruptly.

The differences in the plasma power for the smallest CO_2 admixture can also be explained by this effect. Nonetheless, the conversion rates and energy efficiencies for the various glass plates and catalysts are compared only for the small CO_2 admixture of 0.25 % due to the homogeneous ignition of the plasma in the total electrode area. For the medium and high CO_2 admixtures, no reproducible results can be obtained on the conversion rates for the various glass plates and catalysts. To achieve this, the arrangement of the electrodes must be adapted, which will be described in chapter 5.

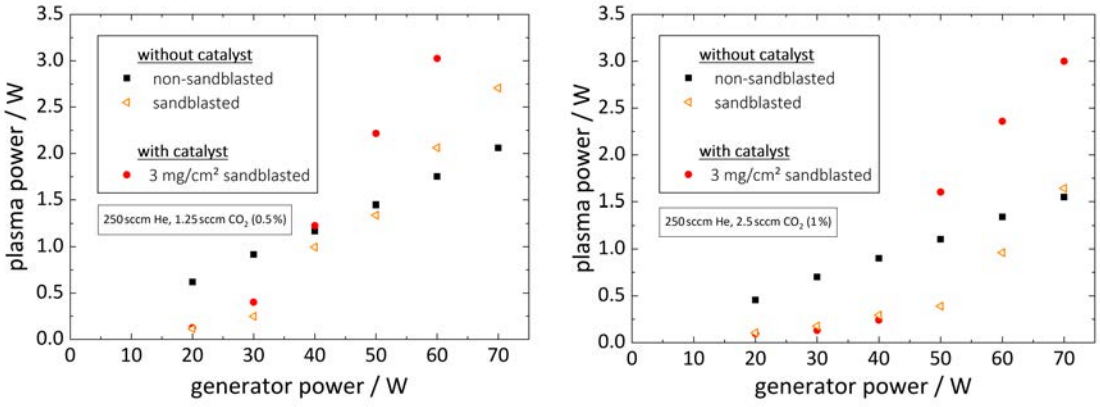

(a) 0.5 % CO_2 admixture. (b) 1 % CO_2 admixture.

Figure 4.3: Plasma power as a function of the generator power for a He flow of 250 sccm with medium (a) and high (b) CO_2 admixture.

Furthermore, the rough surface of the sandblasted glass plates as well as of the glass plates with catalyst can also influence the coupled plasma power. On the rough surface, sinks form which can act as traps for secondary electrons. As a result, fewer secondary electrons enter the plasma and the plasma ignites less efficiently. The electric field on the rough surface can also be changed, which influences the electron energy distribution. This can change the behaviour of the plasma and the plasma power is coupled in a different way. This effect has to be further investigated with the aid of a new plasma chamber design (described in chapter 5) in which the electrodes are arranged in the same way in each experiment.

4.3 Time evolution of the catalysts

The measurement of the absorption spectra for one generator power takes about 5 minutes. Six various generator powers are used for each CO_2 admixture. Thus, the plasma is turned on for at least 90 minutes. To check whether the catalyst changes over time, the absorption spectra are recorded for one hour. For this time measurement, 250 sccm He with 0.25 % CO_2 admixture at a generator power of 50 W is used. The plasma is alternately switched off for two minutes and switched on for ten minutes. The smallest loading on non-sandblasted glass plates and the highest loading on sandblasted glass plates are used as catalysts. In this way, it is investigated whether the conversion rates of the catalyst change over time with varying loadings and whether the effect of sandblasting has an effect on the temporal activity of the catalyst.

The conversion rates of the two catalysts as a function of time are shown in figure 4.4. In each ignition phase (1-5), it can be seen that the conversion rates for both catalysts remain constant. The dashed lines indicate the mean values of both, which are (59.1±2.4) % for the catalyst with the highest loading on sandblasted glass plates and (49.2 ± 4.0) % for the catalyst with the lowest loading on non-sandblasted glass plates. The conversion rates fluctuate slightly around these mean values. In the plasma-off phase, the conversion rates are zero. Furthermore, the conversion rate at the beginning of the catalyst with the lowest loading on non-sandblasted glass plates is significantly lower. This is due to the fact that the plasma must be turned on for a certain time after the first ignition to be fully formed. This is also evident from the coupled plasma power, which is described in the following.

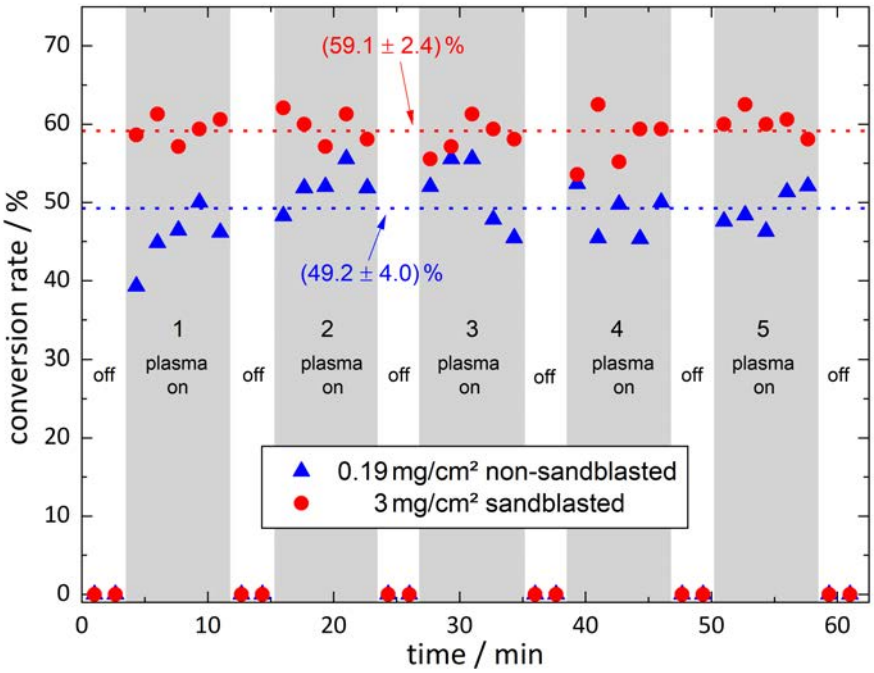

Figure 4.4: Conversion rate for two different catalysts as a function of time. Plasma turned on and off. Numbers match the number of ignition. Dashed lines indicate the mean value of the corresponding conversion rate.

In figure 4.5, the carbon balance corresponding to the sum of CO and CO_2 as a function of time as well as the plasma power for the time measurement are shown. The balance and the plasma power during the time measurement of the catalyst with the highest loading remains constant. This indicates that the plasma catalysis system with the catalyst with the highest loading on sandblasted glass plates is stable over one hour and does not change. In contrast, the balance during the time measurement of the catalyst with the lowest loading on non-sandblasted glass plates decreases while the plasma power increases. This is due to the heating of the system over time, which reduces the overall gas density according to the ideal gas law and increases the coupled plasma power. This effect does not occur for the catalyst with the highest loading, because the system was already turned on for one hour before the time measurement so that it has already heated up.

Nonetheless, the conversion rate remains constant even for the catalyst with the lowest loading on non-sandblasted glass plates so that the systems can be assumed to be constant for the following measurements.

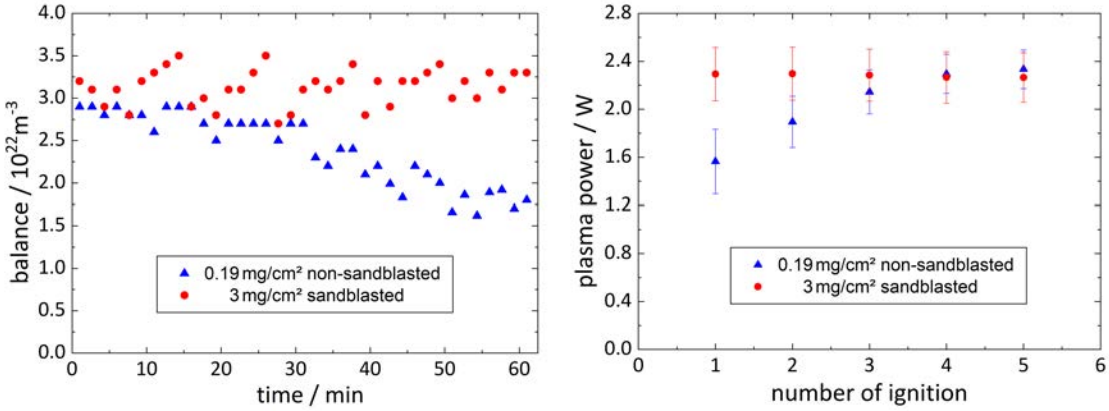

(a) Carbon balance of CO and CO_2.

(b) Plasma power per ignition.

Figure 4.5: Carbon balance and plasma power corresponding to the conversion rates of figure 4.4.

4.4 Conversion rate

This section deals with changes in the conversion rate by the sandblasting of the glass plates and by adding the catalyst. All following measurements were performed with 250 sccm He and 0.25 % CO_2 admixture.

In figure 4.6, the conversion rates as a function of plasma power for sandblasted and non-sandblasted glass plates without catalyst are shown. It can be seen that the conversion rate for the sandblasted glass plates is up to 1.5 W plasma power higher. From a plasma power of 1.75 W, the conversion rate for both glass plates are at the same level and also saturate at the same level of 57 %. Therefore, no clear difference in the conversion rate for the sandblasted and non-sandblasted glass plates can be recognised and it can be assumed that the effect of sandblasting generally has no significant effect on the conversion of CO_2

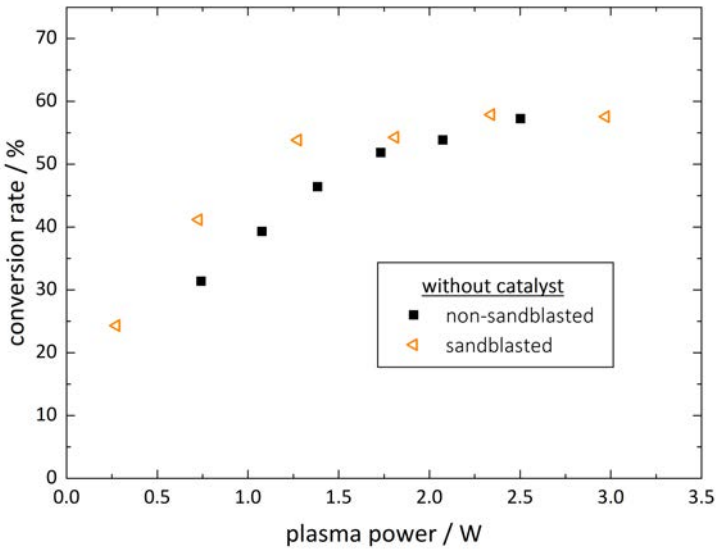

Figure 4.6: Conversion rate as a function of plasma power for sandblasted (orange) and non-sandblasted (black) glass plates without catalyst.

The conversion rates for the catalysts with the smallest loading on sandblasted and non-sandblasted glass plates in comparison to the reference measurement without catalyst on non-sandblasted glass plates are shown in figure 4.7. All three conversion rates show a similar behaviour. They rise from 30 % to around 57 % and saturate at this value. The only noticeable difference is that the plasma power for the last three values of the catalysts is higher as described above (see fig. 4.2).

From this figure it can be conclude that the catalysts with the smallest loading have no discernible influence on the conversion of CO_2. Furthermore, there is no difference between the catalysts on the sandblasted and non-sandblasted glass plates.

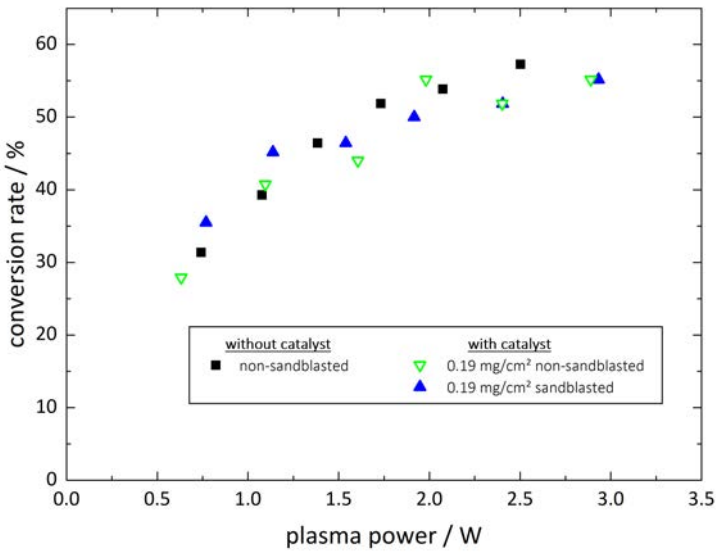

Figure 4.7: Conversion rates for catalysts with smallest loading of 0.19 mg/cm^2 on sandblasted (blue) and non-sandblasted (green) glass plates in comparison with non-sandblasted glass plates without catalyst (black).

In figure 4.8, the conversion rates for catalysts with different loadings as well as the reference measurement without catalyst are shown. The loadings vary between 0.19 mg/cm^2, 0.75 mg/cm^2 and 3 mg/cm^2. All catalysts are applied to sandblasted glass plates.

As describes above, the conversion rate for the smallest loading is equal to the reference measurement without catalyst. For the higher loadings, a clear trend towards higher conversion rates is discernible. The conversion rates for the catalysts with the highest loading are 5 % to 10 % higher than the conversion rates for the reference measurement. For the medium loading, the conversion rates are also higher than for the reference measurement. However, these are lower than the conversion rates for the highest loading. This shows a clear trend: the higher the loading, the higher the conversion rates. Furthermore, the saturation levels for the catalysts with the medium (saturation level of 62 %) and the high (65 %) loadings are higher and are reached earlier than in the reference measurement without catalyst.

Since the effect does not occur for the smallest loading, it can be assumed that a certain loading is necessary to influence the conversion of CO_2. However, three different loadings are not sufficient to investigate this in more detail.

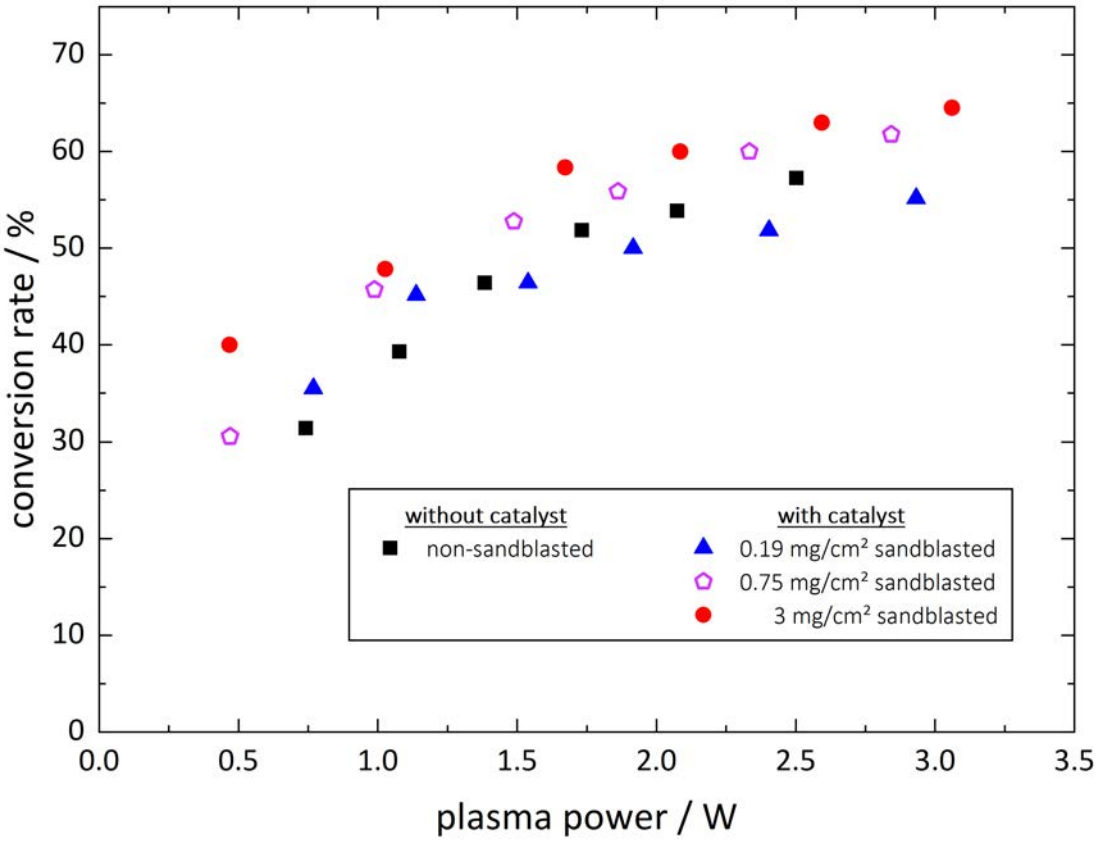

Figure 4.8: Conversion rate for catalysts with loadings of 0.19 mg/cm^2 (blue), 0.75 mg/cm^2 (purple) and 3 mg/cm^2 (red) on sandblasted glass plates as well as the reference measurement without catalyst on non-sandblasted glass plates (black).

4.5 Energy efficiency

Furthermore, the energy efficiency given by equation (2.9) is of interest for the conversion with and without catalyst. The energy efficiencies for each catalyst and the measurements without catalyst on sandblasted and non-sandblasted glass plates are shown in figure 4.9.

For low plasma powers, there is a big difference between the measurements without catalysts on sandblasted and non-sandblasted glass plates. For the sandblasted glass plates, the energy efficiency is initially twice as high. Starting from 1.5 W, the energy efficiencies of the two are at the same level (4 % to 2 %) and show the same behaviour. This corresponds to the conversion rate at which the measurements with the sandblasted glass plates were also initially higher and saturate at the same level as the measurement with non-sandblasted glass plates (see fig. 4.6).

The energy efficiencies of the catalysts with the lowest loading on sandblasted and non-sandblasted glass plates follow the same behaviour as the energy efficiency of the non-sandblasted glass plates without catalyst over the entire range. Thus, analogous to the conversion rate, no differences in the energy efficiency between the reference measurement and the measurement with the smallest loading can be observed.

In addition, the energy efficiencies of the catalysts with the medium and the highest loadings are higher at the beginning compared to the reference measurement. This is due to the higher conversion rates and lower plasma powers of the catalysts at the beginning. For higher plasma powers, the energy efficiencies approach and saturate at the same level.

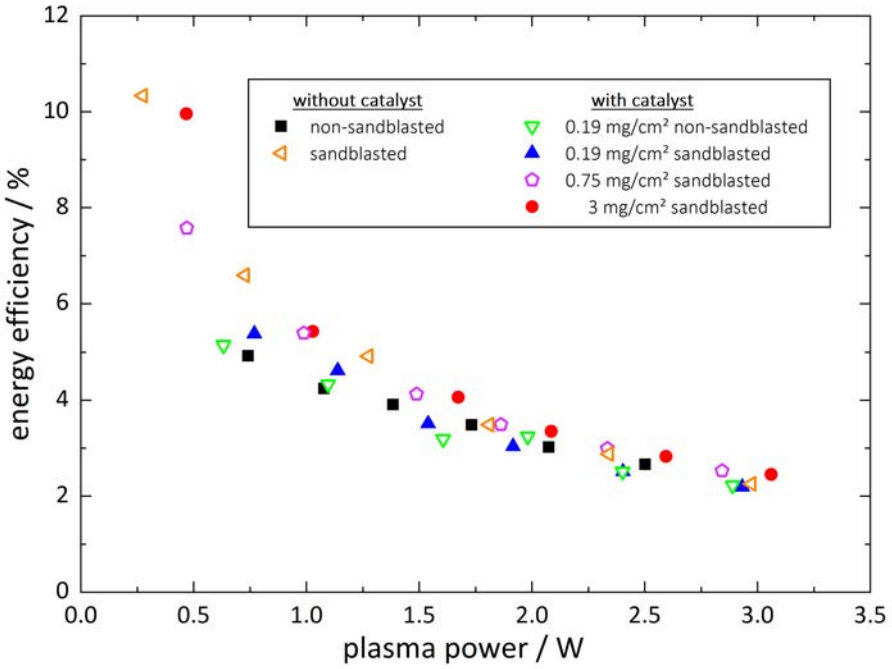

Figure 4.9: Energy efficiency for each catalyst and measurements without catalyst on sandblasted and non-sandblasted glass plates.

4.6 Rotational and vibrational temperatures

In addition to the conversion rates and energy efficiencies, the rotational and vibrational temperatures of CO and CO_2 are of interest. For sake of clarity, the temperatures of the measurements without catalyst on non-sandblasted glass plates and with catalysts with all three loadings on sandblasted glass plates are shown. The temperatures of the other two measurements (without catalyst on sandblasted and with catalyst with the smallest loading on non-sandblasted glass plates) follow the same behaviour as described in the following.

The rotational as well as the vibrational temperatures of CO are shown in figure 4.10. Both temperatures show no clear difference in the use of different catalysts compared to measurement without catalyst. The rotational temperature rises linearly with the plasma power and is in the range of 350 K to 470 K. The rotational temperature indicates the temperature of the gas. As the plasma chamber heats up over time, the range of the rotational temperature is acceptable. The error of the rotational temperature results from the fits to $\pm$ 20 K whereby the rotational temperatures of all measurements can be regarded as equal, considering their confidence range.

The vibrational temperature of CO increases with plasma power and shows the same behaviour for each measurement with or without catalyst. It is in the range of 1200 K to 1800 K. The error of the vibrational temperature by the fit is $\pm$ 150 K. Therefore, the vibrational temperatures of all measurements with and without catalysts can be regarded as equal, considering their confidence range.

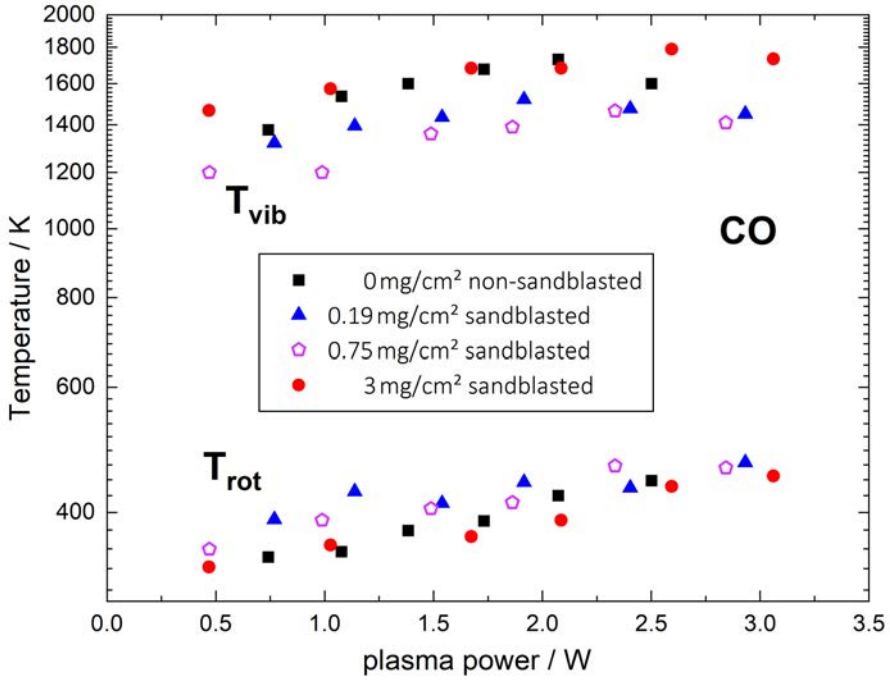

Figure 4.10: Rotational temperature T_{rot} and vibrational Temperature T_{vib} of CO for measurements without catalyst on non-sandblasted glass plates and with catalysts with all three loadings on sandblasted glass plates.

Furthermore, the temperatures of CO_2 are shown in figure 4.11. The rotational temperature T_{rot} (top panel) and the bending temperature T_{vib2} (bottom panel) increase almost linearly from 360 K to 440 K with increasing plasma power and have an error of ± 20 K. The temperature of symmetric vibration T_{vib1} (middle panel) varies in the range from 400 K to 600 K. The determination of this temperature from the fits was very difficult because it has a small influence on the absorption spectrum. Therefore, the error of this temperature is ± 150 K. Finally, the temperature of asymmetric vibration (bottom panel) remains constant for each measurement and is in the range of 600 K and 900 K. The error of this temperature by the fits is ± 100 K.

All in all, no differences between the measurements with and without catalysts can be noticed, considering the confidence range of the temperatures. Therefore, the catalysts have no effects on the temperatures of CO and CO_2. This indicates that the effect of the catalyst does not affect the electronic excitation of the molecules.

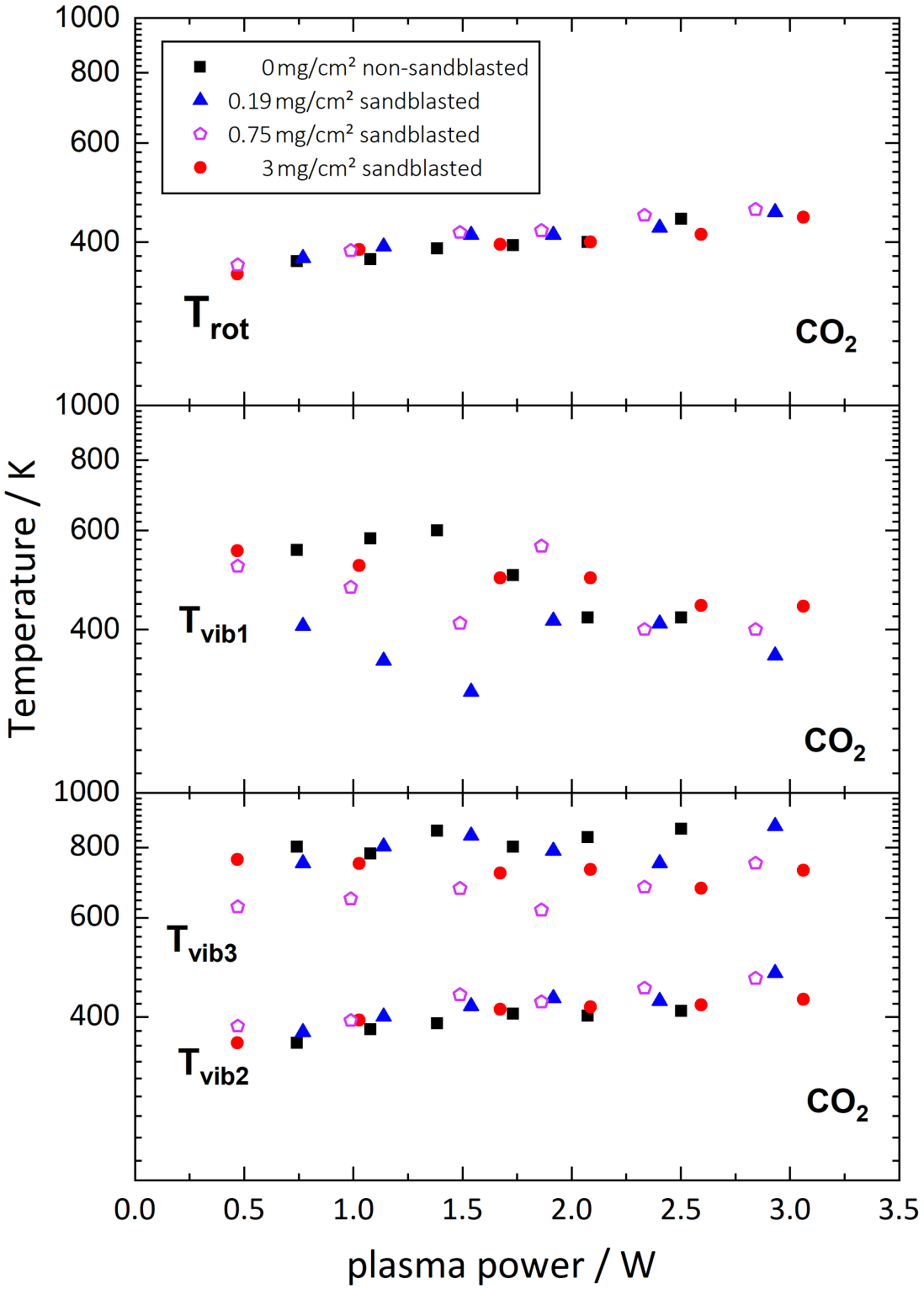

Figure 4.11: Rotational and vibrational temperatures of CO_2. Top panel: rotational temperature T_{rot}. Middle panel: temperature of symmetric stretching T_{vib1}. Bottom panel: temperatures of bending T_{vib2} and asymmetric stretching T_{vib3}.

4.7 Performance of plasma catalysis system

The performance of the plasma catalysis system will be described in the following. This process is shown in figure 4.12. On the left side, the plasma assisted dissociation of CO_2 is illustrated. CO_2 enters the plasma, is dissociated and CO as well as atomic oxygen are formed. The dissociation of CO_2 at the catalyst surface is shown on the right side. The catalyst surface consists of MnO_2 and vacancies. The CO_2 reaches the catalyst surface and binds with an oxygen atom at a vacancy. Afterwards, the CO_2 dissociate and another vacancy binds the CO. The CO then passes into the gas phase and the vacancy is released again.

The last step is the desorption of oxygen. Thermally, this process is the slowest since oxygen is the most stable adsorbate. But in the plasma catalysis system, this process is accelerated by the atomic oxygen from the plasma dissociation. It recombines with the atomic oxygen of the catalyst surface to molecular oxygen. After this step, two CO_2 molecules dissociate to two CO molecules and one molecular oxygen, which corresponds to the total dissociation according to equation (2.7).

Therefore, the combination of a plasma with a catalyst enhanced the CO_2 conversion yielding to higher conversion rates of the plasma catalysis system than the plasma alone. Theoretically, a factor of two in the conversion rate is possible due to the combination of a plasma with a catalyst.

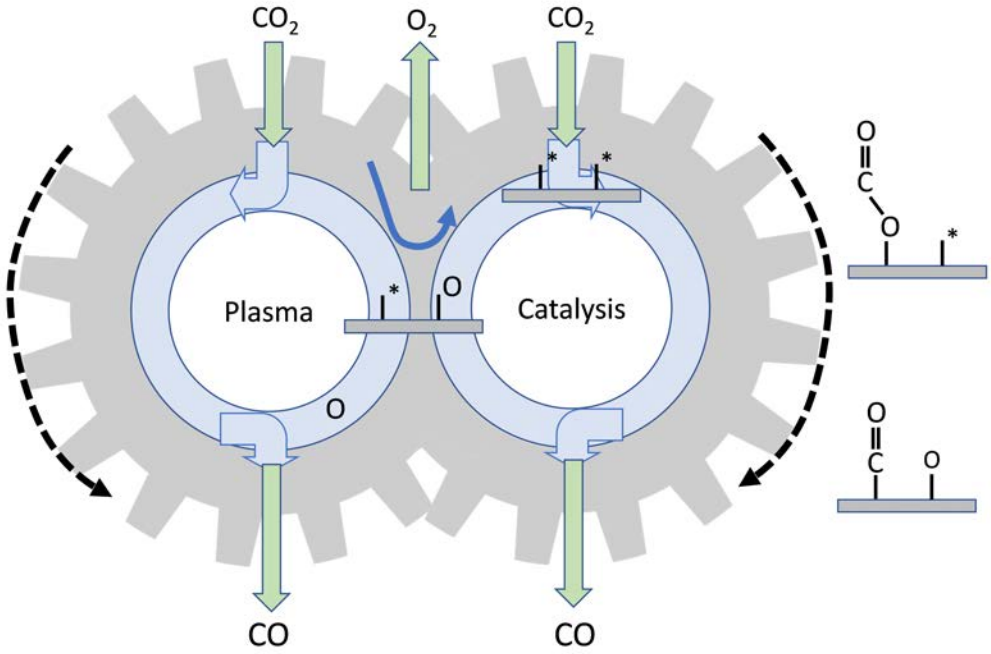

Figure 4.12: Performance of the plasma catalysis system.

This factor can not be observed in these measurements. This is due to the fact that the conversion rate is already high (57 %, see fig. 4.8) for the measurement without catalyst as described above. If the factor were two, the conversion rate would be higher than 100 % for the measurement with catalyst. Therefore, the factor of the catalyst has to be smaller than two for high plasma powers. At low plasma powers, the conversion without catalyst is not yet as efficient and the factor of two in the conversion rate with a catalyst should be recognisable. In order to investigate this in more detail, generator powers below 20 W have to be used if the plasma can still be ignited. Furthermore, higher helium gas flow rates can also be used to reduce the conversion rate without catalyst due to the lower residence time and the factor of two should then be discernible.

5. Summary and outlook

The influence of catalysts on CO_2 conversion in a non-equilibrium atmospheric pressure plasma was investigated. Manganese dioxide (MnO_2) was used as material for the catalysts. The loading of the catalyst material on the glass plates was $0.19\,mg/cm^2$, $0.75\,mg/cm^2$ as well as $3\,mg/cm^2$ and the effect of sandblasting on the conversion was investigated.

The glass plates with catalysts were installed in such a way that the surface of the catalyst was in direct contact with the plasma. The plasma for the medium and high CO_2 admixture could not be ignited homogeneously. This was due to the fact that the electrodes were mounted laterally offset to each other. Nevertheless, the CO_2 conversion for the various catalysts could be compared for the small CO_2 admixture.

It was found that the conversion rates of CO_2 in the plasma jet increase by the use of catalysts. In addition, it was found that the higher the loading of the catalysts, the higher the conversion rate. On the other hand, the smallest loading does not increase the conversion rate. Thus, it can be assumed that a certain loading is necessary to sufficiently influence the CO_2 conversion. However, three different loadings are not sufficient to investigate this in detail and more loadings should be tested. Furthermore, the effect of sandblasting the glass plates has no significant effect on the conversion.

The energy efficiency initially shows higher values for the catalysts with the medium and the highest loadings. This is due to the lower plasma powers and simultaneously higher conversion rates. But for higher plasma powers, all profiles approach and saturate on the same level.

The rotational as well as the vibrational temperatures of CO and CO_2 do not show any changes, considering their confidence range. Thus, the use of catalysts does not affect the electronic excitation and the catalysts enhance the conversion by a surface reaction. Thereby, the plasma dissociation and the catalytic dissociation interact by recombining the free atomic oxygen from the plasma with the bound oxygen atom on the catalyst surface. In this way, the vacancies of the catalyst surface will become free again.

Further measurements have to be carried out to investigate the influence of catalysts on CO_2 conversion in more detail. Generator powers less than 20 W have to be used to investigate the increase of the conversion rate by the catalyst to a factor of two. Alternatively, this could also be investigated with a higher helium gas flow, which significantly reduces the conversion rate whereby the factor of two may be discernible.

In addition, the roughness of the surface can also have an effect on the CO_2 conversion and on the coupled plasma power. In order to investigate this, the roughness of the surface has to be characterised and the conversion rates depending on the roughness have to be analysed. The effect of the loading on the CO_2 conversion has also to be further examined by increasing the variation of the loading.

Moreover, only MnO_2 was used as the catalyst material. Further materials like NiO or Pt can also be promising for catalytic measurements.

Furthermore, the setup of the plasma chamber has to be improved. This is already planned in such a way that the electrodes are countersunk in the macor layer. Thereby, it is guaranteed that the electrodes are arranged in the same way in each implementation. This is necessary to improve the reproducibility of the results. In addition, the new setup has a cooling and heating device for the aluminium main body. Since catalysis is a thermal process, it is particularly important to be able to determine and control the temperature of the catalyst surface.

All in all, the CO_2 conversion is increased by the use of MnO_2 catalysts within the plasma jet without changing the rotational and vibrational temperatures of CO and CO_2. In order to investigate this effect in more detail, further measurements have to be carried out. For this purpose, a new plasma chamber has to be used to obtain reproducible and comparable results.

Bibliography

[1] IPCC 2007: Climate Change 2007: The Physical Science Basis. Contribution of Working Group I to the Fourth Assessment Report of the Intergovernmental Panel on Climate Change, 2007.

[2] A. Bogaerts et al.: Plasma-based conversion of CO2: current status and future challenges. *Faraday Discuss*, 2015.

[3] T. Urbanietz et al.: Non-equilibrium excitation of CO2 in an atmospheric pressure helium plasma jet. *Journal of Physics D: Applied Physics*, 2018.

[4] S. Paulussen et al.: Conversion of carbon dioxide to value-added chemicals in atmospheric pressure dielectric barrier discharges. *Plasma Sources Science and Technology*, 2010.

[5] A. Robby et al.: Carbon Dioxide Splitting in a Dielectric Barrier Discharge Plasma: A Combined Experimental and Computational Study. *ChemSusChem*, 2015.

[6] R. Aerts et al.: In-Situ Chemical Trapping of Oxygen in the Splitting of Carbon Dioxide by Plasma. *Plasma Processes and Polymers*, 2014.

[7] T. Silva et al.: Optical characterization of a microwave pulsed discharge used for dissociation of CO2. *Plasma Sources Science and Technology*, 2014.

[8] A. Vesel et al.: Dissociation of CO2 molecules in microwave plasma. *Chemical Physics*, 2011.

[9] A. Indarto et al.: Conversion of CO2 by gliding arc plasma. *Environmental engineering science*, 2006.

[10] T. Nunnally et al.: Dissociation of CO2 in a low current gliding arc plasmatron. *Journal of Physics D: Applied Physics*, 2011.

[11] L. F. Spencer et al.: Efficiency of CO2 Dissociation in a Radio-Frequency Discharge. *Plasma Chemistry and Plasma Processing*, 2011.

[12] H. Lien-Te et al.: Decomposition of carbon dioxide in the RF plasma environment. *Journal of Chemical Technology & Biotechnology*, 1998.

[13] A. P. S. Foote et al.: Two step vibrational excitation dissociation and the recycling of atomic oxygen in the conversion of CO_2 in atmospheric pressure plasmas. *23rd International Symposium on Plasma Chemistry in Montreal*, 2017.

[14] V. D. Rusanov et al.: The physics of a chemically active plasma with nonequilibrium vibrational excitation of molecules. *Soviet Physics Uspekhi*, 1981.

[15] G. Chen et al.: An overview of CO2 conversion in a microwave discharge: the role of plasma-catalysis. *Journal of Physics D: Applied Physics*, 2017.

[16] Y. Wen et al.: Decomposition of CO2 Using Pulsed Corona Discharges Combined with Catalyst. *Plasma Chemistry and Plasma Processing*, 2001.

[17] D. Mei et al.: Plasma-photocatalytic conversion of CO2 at low temperatures: Understanding the synergistic effect of plasma-catalysis. *Applied Catalysis B: Environmental*, 2016.

[18] L. F. Spencer et al.: CO2 dissociation in an atmospheric pressure plasma/catalyst system: a study of efficiency. *Plasma Sources Science and Technology*, 2013.

[19] F. F. Chen: *Introduction to Plasma Physics and Controlled Fusion*. Plenum Press, New York, 1984.

[20] A. Fridman: *Plasma Chemistry*. Cambridge University Press, 2008.

[21] W. Demtröder: *Experimentalphysik 3: Atome, Moleküle und Festkörper*. Springer-Verlag, 2016.

[22] W. J. Moore: *Grundlagen der Physikalischen Chemie*. Walter de Gruyter, Berlin, 1990.

[23] T. Kozák et al.: Splitting of CO2 by vibrational excitation in non-equilibrium plasmas: a reaction kinetics model. *Plasma Sources Science and Technology*, 2014.

[24] H. Bremer et al.: *Heterogene Katalyse: eine Einführung*. Akademie-Verlag, 1978.

[25] S. T. Oyama et al.: Homogeneous, heterogeneous, and enzymatic catalysis. *Journal of Chemical Education*, 1988.

[26] E.-G. Schlosser: *Heterogene Katalyse*. Verlag Chemie, 1972.

[27] J. M. Hollas: *Moderne Methoden in der Spektroskopie*. Vieweg, 1995.

[28] G. Gaulitz et al.: *Handbook of Spectroscopy*. Wiley-VCH Verlag, 2014.

[29] S.-J. Klose: *CO_2-Conversion in Non-Equilibrium Atmospheric Pressure Plasmas*. MSc thesis. Ruhr-Universität Bochum, 2017.

[30] K. Rügner: *Investigation of surface processes during the growth of thin films from cold atmospheric pressure plasmas*. PhD thesis. Ruhr-Universität Bochum, 2015.

[31] B. L. M. Klarenaar et al.: Time evolution of vibrational temperatures in a CO 2 glow discharge measured with infrared absorption spectroscopy. *Plasma Sources Science and Technology*, 2017.

[32] C. Oberste-Beulmann: *Entwicklung einer Methode zur Beschichtung von Plattenelektroden mit heterogenen Katalysatoren für die oxidative Plasmakatalyse.* BA thesis. Ruhr-Universität Bochum, 2018.

Acknowledgement

Abschließend möchte ich mich herzlich bei allen bedanken, die mich bei der Erstellung dieser Arbeit begleitet und unterstützt haben. Ein besonderer Dank geht dabei an:

- Prof. Dr. Achim von Keudell, der es mir ermöglicht hat diese interessante Arbeit am Lehrstuhl für Experimentalphysik II der Ruhr-Universität Bochum zu erstellen.
- Dr. Marc Böke, der sich zur Übernahme der Zweitkorrektur bereiterklärt hat.
- Theresa Urbanietz, die mich in das Experiment eingewiesen hat, mir immer helfend zur Seite stand und das Korrekturlesen dieser Arbeit übernommen hat.
- Maike Kai und David Steuer, die für eine absolut umwerfende, freundliche und angenehme Stimmung im Büro gesorgt haben und für die zahlreichen spannenden und tiefsinnigen Gespräche.
- Meine Kommilitonen, allen voran Thilo Romba und Jan Hendrik Löwer, welche sich mit mir durch das Studium gekämpft haben und für eine wunderbare Zeit gesorgt haben.
- Die Techniker des Lehrstuhls für Experimentalphysik II, die mir bei technischen Problemen mit dem Experiment umgehend geholfen haben.
- Alle Mitarbeiter des Lehrstuhls für Experimentalphysik II, die für eine tolle und angenehme Arbeitsatmosphäre am Lehrstuhl gesorgt haben und immer hilfreich zur Seite standen.
- Meinen Vater Werner Schüttler, der mir jeden Tag den Rücken freihält, mich aufbaut und für mich ein besonderes Vorbild ist.
- Meine gesamte Familie, welche mich während meines Studiums motiviert und unterstützt hat und insbesondere an meine Tante Ulrike Voß, die mich zur Aufnahme des Physikstudiums bewegt hat.
- Meine Freunde, die für mich immer zur Seite stehen und für wundervolle Momente neben dem Studium sorgen.